BSGF
Earth Sciences Bulletin

Available online at:
www.bsgf.fr

A decade of seismicity in metropolitan France (2010–2019): the CEA/LDG methodologies and observations

Clara Duverger, Gilles Mazet-Roux[*], Laurent Bollinger, Aurélie Guilhem Trilla, Amaury Vallage, Bruno Hernandez and Yves Cansi

CEA, DAM, DIF, F-91297 Arpajon, France

Abstract – We summarize ten years of the French seismicity recorded by the Geophysical and Detection Laboratory (LDG) of the French Alternative Energies and Atomic Energy Commission (CEA) network from 2010 to 2019. During this period, 25 265 natural earthquakes were detected by the LDG and located within metropolitan France and its immediate vicinity. This seismicity contributes to more than 47% of the natural earthquakes instrumentally recorded since 1962 (mainly due to the improvement of network capacity), and includes about 28% of the most significant earthquakes with a magnitude $ML \geq 4.0$. Recent seismic events therefore significantly expand the available national catalogues. The spatial distribution of 2010–2019 earthquakes is broadly similar to the previously recorded instrumental pattern of seismicity, with most of the seismic activity concentrated in the French Alps, the Pyrenees, Brittany, the upper Rhine Graben and the Central Massif. A large part of the seismic activity is related to individual events. The largest earthquakes of the last ten years include the November 11, 2019 Le Teil earthquake with ML 5.4 and epicentral intensity VII–VIII, which occurred in the Rhone valley; the April 28, 2016 La Rochelle earthquake with ML 5.1 and epicentral intensity V, which occurred at the southernmost extremity of the Armorican Massif in the vicinity of the Oléron island; and the April 7, 2014 Barcelonnette earthquake with ML 5.1 and epicentral intensity V–VI, which occurred in the Ubaye valley in the Alps. In 2019, two other moderate earthquakes of ML 5.1 and ML 4.9 stroke the western part of France, in Charente-Maritime and Maine-et-Loire departments, respectively. The recent moderate earthquake occurrences and the large number of small earthquakes recorded give both the potential to revise some regional historical events and to determine more robust frequency-magnitude distributions, which are critical for seismic hazard assessment but complex due to low seismicity rates in France. The LDG seismic network installed since the early 1960s also allows a better characterization of the temporal structure of seismicity, partly diffused and in the form of mainshock-aftershocks sequences or transient swarms. These aspects are important in order to lower the uncertainties associated to seismogenic sources and improve the models in seismic hazard assessment for metropolitan France.

Keywords: seismicity / metropolitan France / national seismic network / bulletins and catalogue / seismic hazard / local magnitude

Résumé – Une décennie de sismicité en France métropolitaine (2010–2019) : les méthodes et observations du CEA/LDG. Cette publication résume dix années de sismicité enregistrée par le réseau de stations du Laboratoire de Détection et de Géophysique (LDG) du Commissariat à l'énergie atomique et aux énergies alternatives (CEA) de 2010 à 2019. Au cours de cette période, 25 265 séismes naturels ont été détectés par le réseau et localisés en France métropolitaine ou jusqu'à 20 km des frontières et des côtes maritimes. Cette décade de sismicité correspond à plus de 47 % des séismes instrumentaux toutes magnitudes confondues enregistrés par le réseau depuis 1962 (en raison de l'amélioration des capacités du réseau), et comprend 28 % des séismes français de magnitude $ML \geq 4,0$. Les événements sismiques récents élargissent donc considérablement les catalogues nationaux disponibles. La répartition spatiale des tremblements de terre naturels de 2010–2019 est globalement similaire à celles des observations instrumentales précédentes, la majeure partie de l'activité sismique étant concentrée dans les Alpes

*Corresponding author: gilles.mazet-roux@cea.fr

françaises, les Pyrénées, la Bretagne, la vallée du Rhin et le Massif central. Une grande partie de l'activité sismique est liée à des événements individuels. Les plus grands séismes des dix dernières années incluent le séisme du Teil du 11 novembre 2019 avec une ML 5,4 et une intensité épicentrale VII–VIII, qui s'est produit dans la vallée du Rhône ; le séisme de La Rochelle du 28 avril 2016 avec une ML 5,1 et une intensité épicentrale V, survenu à l'extrémité sud du Massif armoricain à proximité de l'île d'Oléron ; et le séisme de Barcelonnette du 7 avril 2014 avec une ML 5,1 et une intensité épicentrale V–VI, survenu dans la vallée de l'Ubaye dans les Alpes. En 2019, deux autres séismes modérés de ML 5,1 et ML 4,9 ont frappé l'ouest de la France, en Charente-Maritime et Maine-et-Loire respectivement. Les récentes réalisations de séismes modérés et le grand nombre de petits séismes enregistrés donnent à la fois le potentiel de réviser certains événements historiques régionaux et de déterminer des distributions fréquence-magnitude plus robustes, qui sont cruciales pour l'évaluation de l'aléa sismique mais complexes en raison des faibles taux de sismicité en France. Le réseau sismique du LDG étant installé depuis le début des années 1960, ces données permettent également une meilleure caractérisation de la structure temporelle de la sismicité, en partie diffuse, et sous forme de séquences de répliques ou d'essaims transitoires. Ces aspects sont importants pour diminuer les incertitudes liées aux sources sismogènes et pour in fine améliorer les modèles d'évaluation de l'aléa sismique pour la France métropolitaine.

1 Introduction

The seismic activity in metropolitan France has been systematically documented since the 19th century. As elsewhere, the early earthquake catalogues were first obtained from the compilation of macroseismic testimonies (*e.g.* Perrey, 1875), and later on from a mix of macroseismic and instrumental observations following the deployment of the first permanent seismological stations (*e.g.* Rothé, 1936). The deployment of a first national network in the early 1960s is a game-changer by significantly improving the instrumental detection capacity. Its capacity quickly allowed the systematic association of instrumental parameters to the macroseismic earthquake catalogue. Since then, several national catalogues were built from historical and instrumental observations. Among them, 1) the SisFrance catalogue (Scotti *et al.*, 2004), which is an historical catalogue of macroseismic intensities from the 5th to the 20th century (http://www.sisfrance.net), 2) the SiHeX catalogue (Cara *et al.*, 2015), an instrumental catalogue of natural events recorded from 1962 to 2009 including LDG data, with a homogeneous moment magnitude systematically reported, and 3) the FCAT-17 catalogue (Manchuel *et al.*, 2018), which mixes historical and instrumental catalogues optimized for their use in seismic hazard assessment.

The data acquired by the seismic network of the Geophysical and Detection Laboratory (LDG) of the French Alternative Energies and Atomic Energy Commission (CEA) since 1962 has been systematically documented in seismic bulletins, contributing then to the national catalogue. The weekly bulletins are available online (http://www-dase.cea.fr/) since 2000. This paper synthetizes for the first time the LDG detection and location routines, and describes the evolution of the seismic network and stations in operation. Details are also given on the methodologies developed by the LDG to estimate the magnitudes (ML and MD) and on the attenuation law used for the French territory.

Currently, there is a lack in publication taking into account the annual seismicity after 2009 to update and improve these French reference catalogues. Therefore, we gather here the last decade of seismicity recorded by the LDG network from 2010 to 2019. This will help for a future concatenation and homogenization of a new vintage catalogue useful to seismic hazard assessment. We describe the LDG workflows and illustrate our results with statistics on location and magnitude estimation. Then, as a matter of illustration of the contributions of the catalogue, we focus on the five largest earthquakes of this 10-year period with a description of their source parameters (origin, focal mechanism, uncertainties) in their tectonic context. We also present the temporal seismic activity during that period with a particular focus on the Ubaye and the Maurienne seismic swarms in the Alps, which are still active nowadays. We finally list some implications and perspective of this work in term of seismic hazard assessment for metropolitan France.

2 Data acquisition

2.1 The CEA/LDG seismic network in metropolitan France

The LDG operates a nationwide seismic network currently composed of 43 stations with operational high-gain seismometers (Fig. 1 and Tab. 1). The latter consist of 37 vertical-component short-period (1 s) sensors (ZM500), 5 three-component short-period (1 s) sensors (actually one ZM500 and two HM500 collocated for each site) which have been developed in-house (Larsonnier *et al.*, 2019), and 12 broadband (0.1–120 s) sensors (Kinemetrics STS-2 and Nanometrics Trillium T120) collocated with previous short-period sensors, except for one. It also integrates 5 three-component long-period sensors (sensitive to periods from 1 s down to several hundreds of seconds), which have been developed in the 70's by the LDG in the context of a governmental mission of detection. Later on, within the CTBT (Comprehensive nuclear-Test-Ban Treaty), these sensors have been used to rapidly determine the surface magnitude (Ms) of worldwide nuclear tests, with the use of national contributions only.
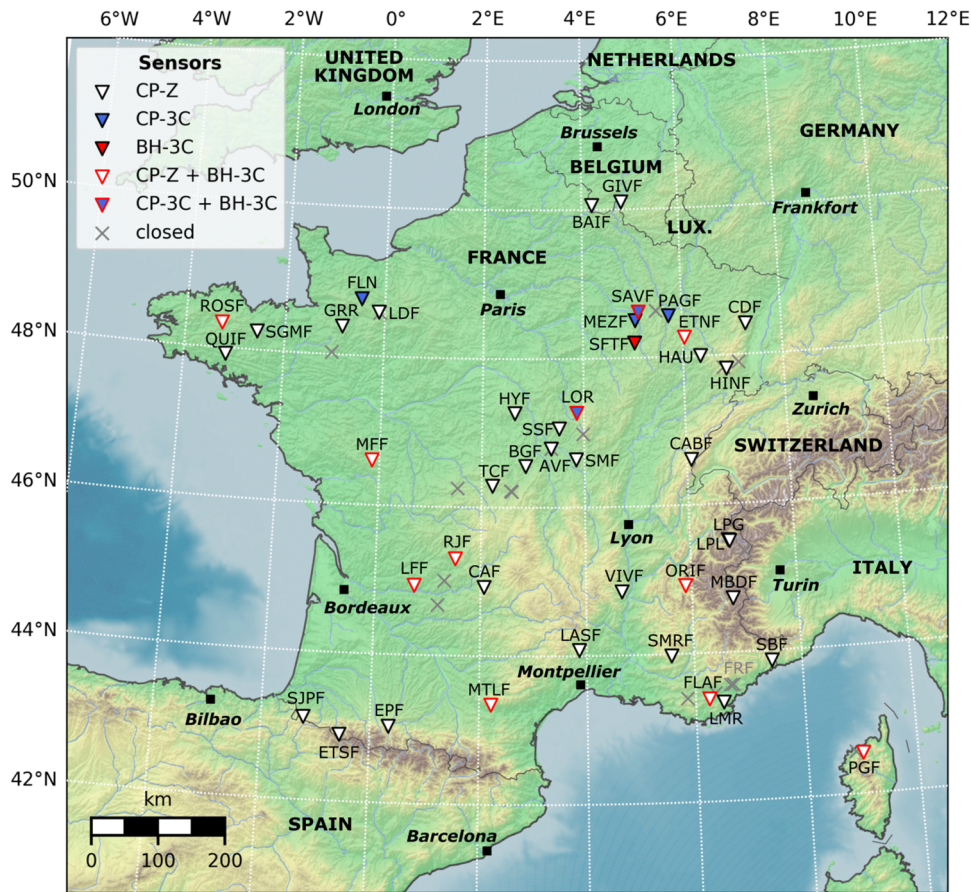
Fig. 1. Map of the LDG seismic network. Triangles represent operational stations in January 2020. White triangles correspond to vertical-component short-period sensors (CP-Z), blue triangles are 3-component short-period sensors (CP-3C), and red triangles are 3-component broadband sensors (BH-3C). CP-Z and BH-3C sensors are collocated at nine stations and represented by white triangles with red borders. CP-3C and BH-3C sensors are collocated at two stations and represented by blue triangles with red borders. During the period 2010–2019, BH-3C sensors were installed at stations SAVF, FLAF and ENTF. Gray crosses represent former stations closed before 2010 except for station FRF, which closed in 2016 (see Tab. S1 for more details). Black squares indicate major cities.

The LDG seismic network is designed to continuously monitor the ongoing earthquake activity down to magnitudes well below the human perception threshold, and to communicate the rapid earthquake information towards the French authorities. This information is sent for magnitude 3.5 and above earthquakes on the metropolitan territory. Earthquake monitoring and information for French overseas territories (*e.g.* French Antilles or Reunion Island) are performed by local seismological centers.

The LDG seismic network is the first and the oldest permanent seismic network installed in metropolitan France (Nicolas *et al.*, 1998). It started in 1962 with the deployment of seven short-period stations: FLN, GRR, LOR, SSF, TCF, LRG and SSC (Figs. 1 and 2). The first five stations aforementioned are still in operation in January 2020. In 2002, the LDG initiated a contract with the ANDRA (French national radioactive waste management agency) by installing three 3-component short-period sensors (MEZF, RFYF and SFTF) in northeastern France, around a site which is likely to host underground high-level radioactive wastes on the long term. ANDRA's main objective was to better characterize the local seismicity and better discriminate between natural and

artificial events. In this area, the station RFYF was removed in 2008 and replaced by another 3-component short-period sensor at PAGF station.

Between 2006 and 2008, broadband seismometers (STS-2) have been co-located with the short-period sensors at six sites (ROSF, MFF, MTLF, LOR, ORIF and PGF) in order to improve their detection and resolution capacity. The latest stations to be opened during the last ten years were SAVF in 2014, FLAF in 2016, and ETNF in 2017, with vertical short-period sensors at first. In 2018–2019, these 3 stations have been supplemented with broadband sensors (Trillium T120). For information, the original 3-component short-period sensor of SFTF station was replaced by a broadband sensor (Trillium T120) in December 2018. The detailed characteristics of each station installed since the LDG seismic network inception, in 1962, are described in the Table S1 and the evolution of the network is summarized in the Figure 2.

In the framework of the French seismological and geodetic network (RESIF, http://www.resif.fr) project, the LDG currently shares real-time data of eight of its stations with the French academic community. Therefore, to comply with RESIF standards, the STS-2 installed in station MFF was replaced by

Table 1. The LDG seismic stations. The table presents some characteristics of the 43 high-gain seismometers of the LDG French national network operational in January 2020. Columns correspond to the station code name, the types of sensor (CP-Z: vertical-component short-period; CP-3C: three-component short-period; BH-3C: three-component broadband) and the geographical location with the French department number between brackets. Apart from station SFTF, each station equipped with a broadband sensor is also equipped with a short-period sensor.

Code	Sensors	Station location
AVF	CP-Z	Avril-sur-Loire (58)
BAIF	CP-Z	Baives (59)
BGF	CP-Z	Louroux-Bourbonnais (03)
CABF	CP-Z	Chapelle-des-Bois (25)
CAF	CP-Z	Sousceyrac-en-Quercy (46)
CDF	CP-Z	Belmont (67)
EPF	CP-Z	Labastide (65)
ETNF	CP-Z, BH-3C	Estrennes (88)
ETSF	CP-Z	Etsaut (64)
FLAF	CP-Z, BH-3C	Flassans-sur-Issole (83)
FLN	CP-3C	Athis-Val de Rouvre (61)
GIVF	CP-Z	Charnois (08)
GRR	CP-Z	Colombiers-du-Plessis (53)
HAU	CP-Z	La Chapelle-aux-Bois (88)
HINF	CP-Z	Sewen (68)
HYF	CP-Z	Humbligny (18)
LASF	CP-Z	Sainte-Croix-de-Caderle (30)
LDF	CP-Z	Saint-Sauveur-de-Carrouges (61)
LFF	CP-Z, BH-3C	Sainte-Foy-de-Longas (24)
LMR	CP-Z	Le Plan-de-la-Tour (83)
LOR	CP-3C, BH-3C	Lormes (58)
LPG	CP-Z	La Plagne Tarentaise (73)
LPL	CP-Z	La Plagne Tarentaise (73)
MBDF	CP-Z	Château-Ville-Vieille (05)
MEZF	CP-3C	Maizières (52)
MFF	CP-Z, BH-3C	Saint-Martin-du-Fouilloux (79)
MTLF	CP-Z, BH-3C	Saint-Denis (11)
ORIF	CP-Z, BH-3C	Oris-en-Rattier (38)
PAGF	CP-3C	Champougny (55)
PGF	CP-Z, BH-3C	Pioggiola (2B)
QUIF	CP-Z	Quistinic (56)
RJF	CP-Z, BH-3C	Saint-Bonnet-l'Enfantier (19)
ROSF	CP-Z, BH-3C	Trémargat (22)
SAVF	CP-3C, BH-3C	Savonnières-en-Perthois (55)
SBF	CP-Z	Sospel (06)
SFTF	BH-3C	Sexfontaines (52)
SGMF	CP-Z	Le Méné (22)
SJPF	CP-Z	Saint-Michel (64)
SMF	CP-Z	Mont (71)
SMRF	CP-Z	Simiane-la-Rotonde (04)
SSF	CP-Z	Saxi-Bourdon (58)
TCF	CP-Z	Toulx-Sainte-Croix (23)
VIVF	CP-Z	Saint-Julien-le-Roux (07)

Trillium T120 and broadband sensors (Trillium T120) have been added to stations RJF and LFF in 2019. To complete the RESIF network, the LDG committed to install and share the real time data of eight additional stations by the end of 2021.

Finally, five LDG stations (BAIF, CABF, EPF, QUIF and SMFF) are also equipped with an accelerometer (Kinemetrics EpiSensor ES-T or GeoSIG AC23), whose real time data are made available to the scientific community through the French strong-motion network (RAP, http://rap.resif.fr). These last stations are planned to be replaced in the next years by more recent technologies.

2.2 Seismological bulletin procedure

The continuous waveforms recorded by the LDG stations are analyzed in real-time and scrutinized by an analyst. The aim of this procedure is to identify any seismic event recorded on the LDG seismic network. Seismic signals associated to teleseismic phases are discarded. When an event is observed, seismic phases (Pg, Pn, Sg and Sn) are manually picked by the analyst and the event is then located *via* an earthquake location algorithm developed by the LDG (Nicolas *et al.*, 1998). This location technique is based on the Geiger (1910) least square method using a velocity model and an attenuation law to determine the location magnitude (M_L) that are described in the next section.

Furthermore, the locations of events are also determined using the waveforms of several tens of additional stations operated by other French and foreign seismic networks *via* RESIF (http://seismology.resif.fr/) and GEOFON (http://geofon.gfz-potsdam.de/) SeedLink servers. The signals of the closest stations are analyzed by the operators (phase pickings). This helps to better constrain the epicentral location and the hypocentral depth by adding as many close stations as possible. For earthquakes located in the vicinity of the national borders (in or outside the French metropolitan territory), the analyst integrates additional phases picks obtained from other French regional networks or from seismological centers in neighboring countries. The list of networks which are considered is given in the Table S2. Only station codes that are registered at the International Registry of Seismograph Stations (http://www.isc.ac.uk/registries) are taken into account. On average, during the period 2010–2019, 57% of the picked phases used in the location process are read on LDG stations. The final location, hypocentral depth and magnitude of each event are refined and validated by a senior seismologist who is also in charge of the discrimination between natural and artificial events.

The LDG seismic bulletins are published on a weekly basis in GSE2.0 format on the CEA/DASE website (http://www-dase.cea.fr). GSE bulletins only contain natural events and only show the picks and amplitudes measured on the records of the LDG stations. The full bulletin information (with picks of foreign stations) is finally shared with the French Central Seismological Office (BCSF, http://www.franceseisme.fr/) in QuakeML1.2 format. The BCSF receives seismic bulletins from several French regional seismic networks and is in charge of merging them and making the results available to the French seismological community.

2.3 Rapid earthquake information

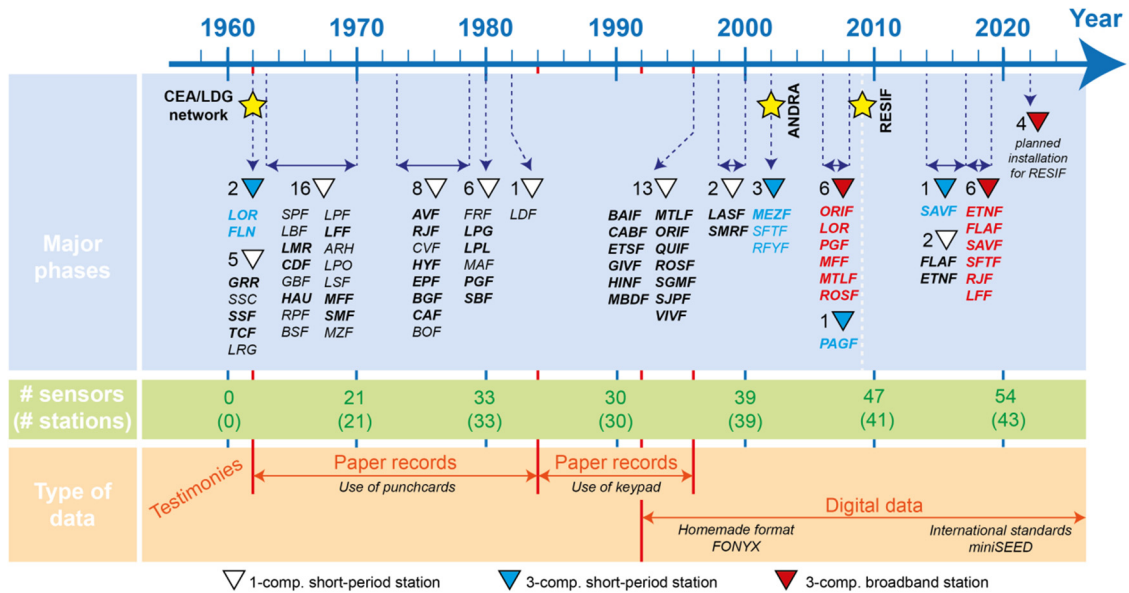The LDG is also in charge of rapidly locating magnitude 3.5 and above earthquakes in the metropolitan territory and

Fig. 2. Chronological evolution of the LDG seismic network and technologies. Blue panel presents the major phases of the LDG seismic network evolution with station and sensor installations. Green panel presents the evolution of number of sensors and number of stations between parentheses, at the network inception (in 1962) and at the end of each decade. Orange panel presents the evolution of type of data. Yellow stars indicate the birth of networks/projects. White triangles correspond to vertical-component short-period station. Blue triangles represent 3-component short-period stations. Red triangles represent 3-component broadband stations. Station names are in bold if they are still running in January 2020. Red names are duplicates since broadband sensors are collocated with short-period sensors, except for SFTF for which the 3-component sensor has been removed and replaced in 2018 by a broadband sensor, alone.

informing its authorities (*e.g.* civil protection services, Ministry of interior). To ensure this mission, the LDG developed an automatic earthquake detection and location system based on STA/LTA (short term average/long term average) detectors implemented on the 43 short-period seismic stations. STA and LTA windows are 10 s and 600 s long respectively and a seismic alert is triggered as soon as the STA/LTA ratio exceeds 5 for at least 13 stations. Automatic detections are transmitted to a seismologist on call who validates the source parameters and disseminates the earthquake information to the end-users. These actions are performed remotely through a VPN. Automatic detection and manually disseminated earthquake locations are also made available on the CEA/DASE website.

2.4 Evolution of data measurements

The tools used to analyze seismic signals at the LDG have obviously evolved over time (Fig. 2). This section retraces the key steps of their evolution, which impact the quality and the processing of data over time and have to be kept in mind for data interpretation.

From 1962 to 1984, amplitudes of seismic signals were measured directly on seismogram papers (Fig. 2). Data were then transferred to the database thanks to punch cards. From 1984 to 1992, amplitudes were still measured on papers but keypad was used to save them in the LDG database. Digital records were acquired since the beginning of 1992, changing the way to measure amplitudes on seismic signals. In 1996, the LDG operated a complete transition from analog to digital acquisitions (Fig. 2). For this purpose, it developed its own

seismic data format (named *FONYX*). Since 2001, the data acquisition processing and software have not significantly evolved. The LDG is currently involved in another transition, using formats and protocols inherited from its activities within the CTBT context and compatible with international standards in terms of seismic data (miniSEED), metadata (QuakeML, FDSN StationXML) and protocols (SeedLink, ArcLink).

3 Waveform analysis and models

3.1 Event discrimination

Seismic activity recorded in metropolitan France comprises natural seismotectonic activity as well as significant human activity. Differentiating natural tectonic earthquakes from other events is therefore important to clean the LDG bulletins in order to build the national earthquake catalogue.

3.1.1 Methodology

Event type discrimination can be a difficult task. It generally needs a bundle of consistent evidences. The discrimination process mostly relies on the analysts' and on the experts' experience. As most of the mining activity in France has stopped during those last decades, most of the non-natural events are now quarry blasts. In most cases seismic signals generated by a quarry blast strongly differ from the ones generated by an earthquake (Figs. S1 and S2). Quarry blasts generate very weak S-waves but generally strong low frequency surface waves, which can be relatively easy to identify. The S-waves caused by quarry blasts are depleted in high frequencies. Another criterion is that quarry blasts occur,
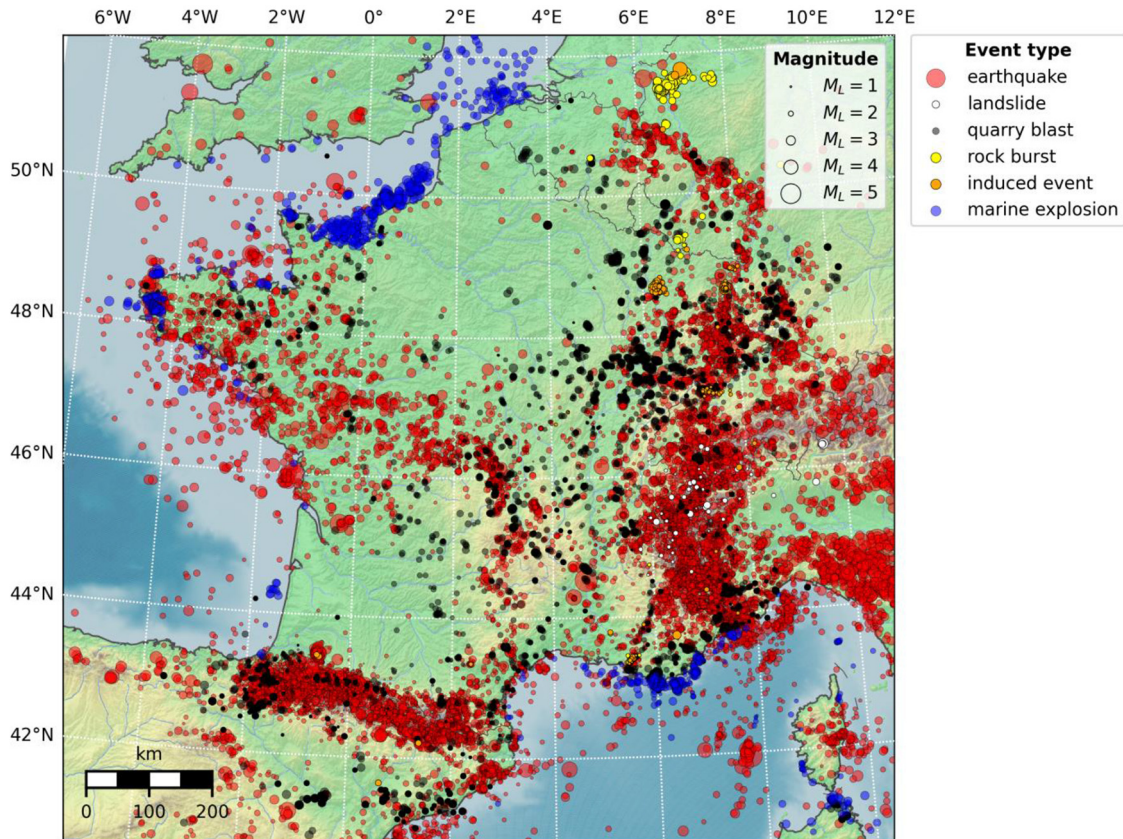
Fig. 3. Epicenters of events recorded by the LDG from 2010 to 2019. Different types of events are recorded in metropolitan France: earthquakes (red), landslides (white), suspected rock bursts (yellow), known or suspected quarry blasts (black), suspected induced events (orange), marine explosions (blue). Only natural earthquakes are exhaustive. When discriminated, anthropogenic events are usually not located so only few of them are represented on this map.

for a vast majority of them, during working hours and during working days although some quarries can remain active during the weekend. A superficial hypocentral depth, as long as it is well constrained, can be an additional clue of an explosive event. The LDG instruments also record offshore marine explosions (Fig. S3) generated by defusing old ammunition by the military authorities near the coasts of the British Channel, the Atlantic Ocean and the Mediterranean Sea. Confirmations of their occurrences are sometimes provided by the authorities.

In addition, within non tectonic events we distinguish the suspected induced events like the ones potentially caused by geothermal activities (*e.g.* near Strasbourg) or gas storage (*e.g.* near Nancy), and the suspected rock bursts due to mines exploitation (*e.g.* in Saar coal mining basin). It is important to notice that the identification of an induced event or a rock burst is a subjective task and these event types are always considered as "suspected". As the seismic signal of an induced event is often similar to the one of a tectonic event, we generally consider that an event is induced when its hypocenter is very superficial and its location falls close to a geothermal power plant for example. We also use the information about event type that is published on other seismological centers websites (*e.g.* BCSF-RéNaSS, https://renass.unistra.fr/, for induced events near Strasbourg).

As for landslides, they are concentrated in the Alps, and not only concern rock falls but also snow avalanches (Fig. S4).

Nonetheless, the LDG almost never receives any confirmation of the occurrence of an actual landslide. Confirmations can however be found in scientific publications. For example in 2011, four detected rock avalanches near Chamonix occurred on September 11 (08:14 UTC) and 12 (05:39 and 05:43 UTC), as well as on October 30 (06:12 UTC). These events were caused by renewed slope failures on the west face of the Aiguille du Petit Dru (Deichmann *et al.*, 2012).

3.1.2 Results

Figure 3 shows all seismic events detected and located by the LDG between 2010 and 2019 in a geographic rectangle area ([40°N; 53°N] and [6°W; 12°E]) encompassing metropolitan France and its surrounding regions. This represents a total of 50 128 seismic events from which 42 694 (85.1%) are identified as tectonic earthquakes. The rest is composed of known or suspected quarry blasts (9.9%), marine explosions (2.1%), suspected earthquakes (1.2%) when the signal-to-noise ratio is too low to confirm its origin, suspected induced events (1.1%), suspected rock bursts (0.4%) and landslides (0.2%). It is important to notice that this catalogue is far from being exhaustive in terms of non-natural (*i.e.* anthropogenic) events as their location processing is not systematic. Except for north-eastern France where the CEA is committed to report any type of seismic event to the ANDRA, anthropogenic

Table 2. The LDG velocity model. This 1-D velocity model is used for seismic event location in metropolitan France at the CEA. It is also used to perform moment tensor inversions of earthquakes presented in this paper (see Sect. 4.3). Columns are the number of the layer, the thickness (h in km), the P-wave velocity (Vp in km.s^{-1}), the S-wave velocity (Vs in km.s^{-1}), the density (ρ), the quality factor for P-waves (Qp) and for S-waves (Qs).

Layer	h (km)	Vp (km.s^{-1})	Vs (km.s^{-1})	ρ	Qp	Qs
1	0.9	3.00	1.73	2.7	200	61
2	25.0	6.03	3.56	2.7	300	128
3	500.0	8.16	4.65	3.3	1000	500

events identified in other parts of the territory are generally removed from the processing.

Since the beginning of the LDG seismic network in 1962, the LDG catalogue contains 89 836 natural tectonic earthquakes. Then, earthquakes recorded in the last 10 years represent more than 47% of the complete earthquake catalogue. This is mainly due to the improvement of network capacity and the resulting lowering of completeness magnitude. It means that the seismicity recorded in the most recent years is also essential to better constrain seismic activity on metropolitan France during the instrumental period and therefore to help in assessing the probabilistic seismic hazard on the French territory.

3.2 Location

3.2.1 Methodology

The seismic records are all integrated into the home-made LDG acquisition-processing software suite. Preliminary hypocenter locations are performed by the analysts but the final arrival times and source parameters are subsequently reviewed by a seismologist. A 1-D three-layer velocity model (Veinante-Delhaye and Santoire, 1980 and references herein) is used for routine localization processing. This model, called LDG model, is an average velocity model determined for the metropolitan France and its surrounding regions. It was defined using the Pg, Sg, Pn, and Sn phases of a series of 50+ well-identified earthquakes in France that were localized by an extensive number of seismic stations external to the LDG network (Veinante-Delhaye and Santoire, 1980). The LDG model is composed of two layers representing the crust and one additional layer for the upper mantle (Tab. 2). The crust consists of a thin sedimentary subsurface layer (0.9 km) above a thick continental crust (25 km) with an average ratio between the P- and S-wave velocities of 1.69. The Moho discontinuity is considered at 25.9 km depth.

In order to test this 1-D velocity model on recent records, we collect phase residuals from earthquakes recorded by the LDG network between 2010 and 2019. The distribution of Pg and Sg time residuals reveals that the observed arrival times are globally consistent with the LDG model, following normal distributions (Figs. S5a and S5b). Moreover, the average Vp/Vs ratio is estimated at 1.69 using Ts–Tp time differences of last decade earthquakes (Fig. S5c). This value matches with the theoretical Vp/Vs ratio used in the continental crust of the LDG model at national scale. The higher residuals in times and the outliers on the Wadati diagram (Fig. S5) certainly

correspond to events from specific regions where the LDG model (national average) is not completely adapted. It would then be interesting to develop regionalized 1-D velocity models, thanks to the substantial increase in seismic records, to better constrain earthquake locations.

3.2.2 Location accuracy

In this part, we assess the quality and the accuracy, when possible, of the locations of natural earthquakes occurred from 2010 to 2019, characterized by a magnitude ML and located either in French metropolitan territory (which includes Corsica) or not further than 20 km of the French borders or coastlines. This represents a total of 25 265 earthquakes (Tab. S3).

Figure 4 shows the distribution of several metrics, which are commonly used in seismic location accuracy analysis: the number of stations and the number of phases used in the location process, and the size of the 95% confidence error ellipse. We complement this analysis with metrics based on the network geometry such as the primary and secondary azimuthal gaps. Finally, we also consider the distance to the closest station, which is rather an indicator of the quality of the hypocentral depth.

As a result, 90% of the locations of ML $\geq$ 1.0 earthquakes are obtained using six stations or more, and 12 phases or more (the median values being 15 stations and 30 phases respectively). The minimal epicentral distance is lower than 55 km for 90% of the events. 90% of the locations have a major semi-axis of the confidence ellipse lower than 4.7 km with a median value of 1.8 km. As the primary and secondary azimuthal gaps give a better estimate of the quality of a location (Bondár *et al.*, 2004), our dataset shows 90% of the locations with a primary and secondary azimuthal gaps lower than 222° and 256° respectively (with median values of 109° and 133° respectively).

However, the error ellipses can be deceptive to assess the location quality, and the two azimuthal gaps are not enough to estimate the accuracy. Therefore, Bondár *et al.* (2004) described a set of criteria based on the network geometry and the number of stations which ensures that the location is accurate within 5 km with a 90% confidence level (Tab. S4). If those criteria are satisfied, the location is called a GT5 (GT standing for Ground Truth). The confidence level of 90% (instead of 95%) comes from the fact that the homogeneity of the spatial distribution of stations is not taken into account in the GT5 criteria.
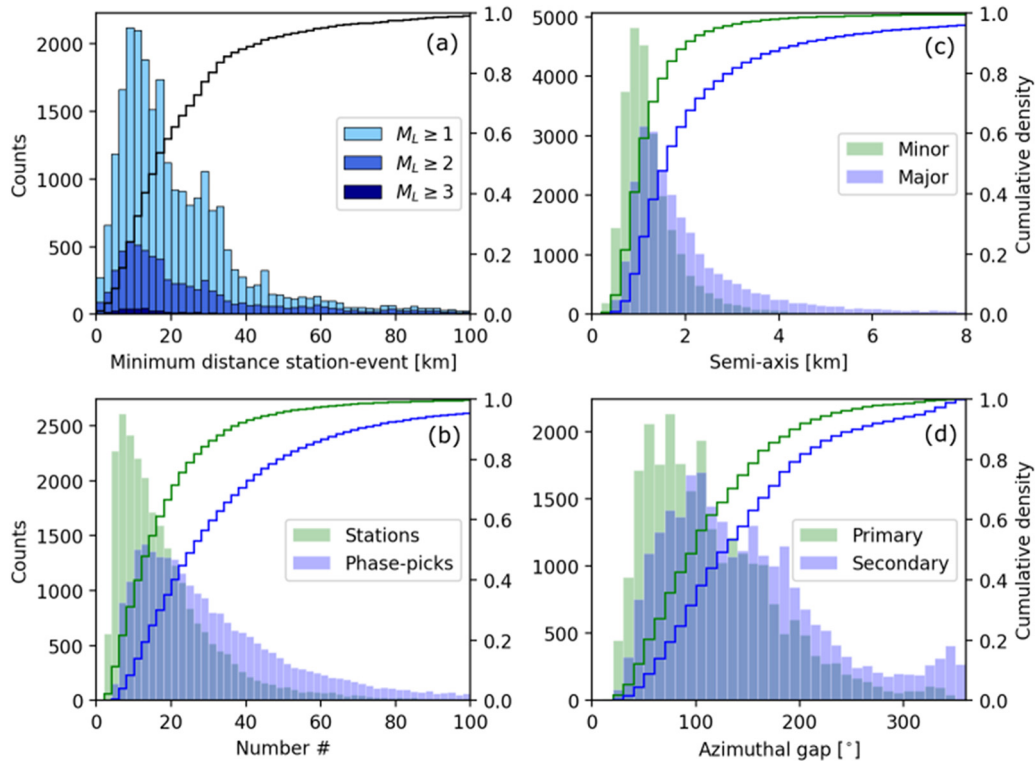
Fig. 4. Statistics on location parameters. Data consist in earthquakes recorded between 2010 and 2019 and located not further than 20 km form the French borders or coastlines. Subplots represent histograms and cumulative density for the considered parameter. (a) Distance between the epicenter and the closest station, in kilometers. Histograms are represented for three magnitude classes: ML ≥ 1 (light blue), ML ≥ 2 (royal blue), ML ≥ 3 (dark blue). The black curve represents the cumulative density of all earthquakes with a ML. (b) Minor and major semi-axis of the 95% confidence error ellipse, in kilometers. (c) Number of stations and number of picking phases. (d) Maximum primary and secondary azimuthal gap, in degrees.

We apply these criteria to our dataset for earthquakes of ML ≥ 3.0 and found that 61% of them satisfy the GT5 criteria defined in the Table S4. Belinić and Markušić (2017) showed that the criterion on the closest station is useful to constrain the hypocenter depth but does not really influence the accuracy of the location. Therefore, if we discard this latter criterion, the ratio of GT5 locations in the 2010–2019 bulletins for ML ≥ 3.0 reaches 76%. Moreover, Belinić and Markušić (2017) statistically determined their own GT5 criteria, for Croatia, based on a set of reference events and showed that Bondár *et al.* (2004) criteria are finally very restrictive and that the actual number of GT5 locations in their bulletin was higher.

Concerning the hypocentral depth, a necessary (but not sufficient) condition to determine a reliable depth with a local network (*i.e.* without depth phases) is that the closest station should not be further that two times the hypocentral depth (*e.g.* Chatelain *et al.*, 1980). This condition is often difficult to achieve for most of the seismic networks. As a consequence, in the case of a loose network, the hypocentral depth is rarely well constrained and finally often corresponds to a default depth which is output by the location algorithm. In our dataset, 26% of the earthquakes get at least one station which is close enough (< 30 km) to constrain the hypocentral depth according to the GT5 criteria. This ratio reaches 31% for earthquakes of ML ≥ 3.0. When the location algorithm fails in determining

a free depth, it tries several default depths (*e.g.* 2, 5, 10 km) and chooses the one that corresponds to the lowest RMS. Furthermore, the analyst may also try other depths that can further improve the RMS. In such a case, the depth is considered "forced". On the period 2010–2019, the earthquakes for which the depth is forced represent 13% of the total.

Other GT criteria like the ones based on Bondár and McLaughlin (2009) will be implemented in our dataset and are therefore not presented here. The final objective at the LDG is to assign quality factor (*e.g.* from A to D) to each location, which could be helpful for bulletin and catalogue users in order to flag very accurate locations as well as very poorly constrained ones. Finally, it is important to notice that the ratios of GT5 and of well constrained hypocentral depth should increase in the coming years as the number of stations, especially the ones installed by the end of the RESIF deployment, should keep on increasing.

3.3 Magnitudes

3.3.1 Local magnitude ML

3.3.1.1 The LDG definition

The historical definition of the local magnitude ML by the LDG dates from 1977 and is described as the following:

Table 3. The LDG attenuation law. Tabulated coefficients of the attenuation of S-waves (Q_0) with epicentral distance (Δ) in kilometers.

Δ (km)	$Q_0(\Delta)$	Δ (km)	$Q_0(\Delta)$	Δ (km)	$Q_0(\Delta)$	Δ (km)	$Q_0(\Delta)$
95	1.60	445	2.50	795	3.13	1145	3.62
145	1.80	495	2.60	845	3.20	1195	3.70
195	2.00	545	2.70	895	3.28	1245	3.75
245	2.10	595	2.80	945	3.35	1295	3.80
295	2.20	645	2.90	995	3.40	1345	3.85
345	2.30	695	3.00	1045	3.48	1395	3.90
395	2.40	745	3.05	1095	3.55	1445	3.90

$$ML_{LDG} = log_{10}\left(\frac{A}{G}\right) + Q_0(\Delta) + C_s,$$

where
- A is the peak-to-peak amplitude in millimeters, measured on the historical LDG acquisition chain (short-period sensor, amplification and paper record (SEFRAM) in the 0.3–7 Hz frequency band) for the Sg, Sn or Lg wave train;
- G is the total gain of the acquisition chain at 1 Hz in millimeters per angstrom (1 Å $= 10^{-10}$ m);
- $Q_0(\Delta)$ is the attenuation curve for Sn or Sg/Lg waves as a function of epicentral distance. It was obtained experimentally with LDG earthquake records after the 1976–77 Friuli seismic crisis (eastern Italian Alps). The values of this attenuation curve are tabulated every 50 km from 95 km to 1445 km according to Table 3.
- C_S is a station correction (statistically determined).

Since the use of computer means, this definition has been amended as follows: considering that the measurement on paper recording stemming from velocity seismometer – without any distortion other than 0.3–7 Hz filtering – is close to the velocity of the ground in this frequency band, we can rewrite the previous equation as follow:

$$ML_{LDG} = log_{10}(V) + Q_1(\Delta) + C_s,$$

where
- V is the maximum peak-to-peak amplitude of the ground velocity (expressed in micrometers per second) in the 0.3–7 Hz frequency band, for the Sn or Sg/Lg wave trains;
- $Q_1(\Delta)$ is a mitigation function adapted from the initial formula:

$$Q_1(\Delta) = Q_0(\Delta) - log_{10}\left(\frac{2\pi}{100\sqrt{2}}\right) \approx Q_0(\Delta) + 1.35.$$

By extension, we can also use an equivalent formulation if we replace the velocity by the displacement (*e.g.* Marin *et al.*, 2004):

$$ML_{LDG} = log_{10}\left(\frac{D}{T}\right) + Q_2(\Delta) + C_s,$$

where
- D is the maximum peak-to-peak amplitude of the ground velocity converted in displacement (expressed in nanometers) in the 0.3–7 Hz frequency band, for the Sn or Sg/Lg wave trains;
- T is the corresponding period of the phase measured in seconds;
- $Q_2(\Delta)$ is adapted from the initial formula as:

$$Q_2(\Delta) = Q_0(\Delta) - log_{10}\left(\frac{10}{\sqrt{2}}\right) \approx Q_0(\Delta) - 0.85.$$

For information, the factor 10 comes from the gain expressed in millimeters per angstrom while the displacement is in nanometers and the factor $\sqrt{2}$ is the correction to be made to take into account the sensor response at 1 Hz. Please note that this is not equivalent to the maximum peak-to-peak value of the ground displacement in the same frequency band. We also give the last relation between $Q_2(\Delta)$ and $Q_1(\Delta)$ for information:

$$Q_2(\Delta) = Q_1(\Delta) - log_{10}\left(\frac{1000}{2\pi}\right) \approx Q_1(\Delta) - 2.20.$$

These three formulations of the tabulated attenuation law, $Q_0(\Delta)$, $Q_1(\Delta)$ and $Q_2(\Delta)$, are represented in Figure S6.

The attenuation law for metropolitan France has also been approximated in 1998 by the LDG as a function of the epicentral distance (Δ) including a geometrical spreading correction term and an anelastic attenuation term such that:

$$B(\Delta) = b_1 log_{10}(\Delta) + b_2\Delta,$$

where $b_1 = 0.84 \pm 0.01$ and $b_2 = 0.00102 \pm 0.0002$. This analytical relation was obtained using more than 54 000 amplitude measurements for significant earthquakes recorded at a minimum of five LDG stations between 1990 and 1995. To compare the attenuation law under the analytical form and the tabulated form, one needs to add a constant depending on the formulation used:

$$B(\Delta) = Q_0(\Delta) - log_{10}\left(\frac{2\pi}{10}\right) \approx Q_0(\Delta) + 2.20,$$

$$B(\Delta) = Q_1(\Delta) - log_{10}\left(10\sqrt{2}\right) \approx Q_1(\Delta) - 1.15,$$

$$B(\Delta) = Q_2(\Delta) - log_{10}\left(\frac{2\pi\sqrt{2}}{100}\right) \approx Q_2(\Delta) + 1.35.$$

The two empirical attenuation laws (tabulated Q(Δ) and analytical B(Δ)) are still compatible with recent records from 2010 to 2019 at national scale (Fig. S6).

Only stations with epicentral distances greater than 95/100 km (100 km before March 25, 2003, 95 km after) are considered for the magnitude determination in order to avoid source and path effects. The final magnitude corresponds to the mean value of individual station magnitudes. Moreover, in 1977, the LDG has demonstrated that the body-wave magnitude (mb) from ISC is equivalent to the local magnitude (ML) from the LDG:

$$ML_{LDG} = mb_{ISC} \pm 0.3.$$

It has to be noted that the ML calculation at the LDG has not been modified from its historical definition in order to keep a consistency in the database through years. However, several technological changes impacted the ML estimation (Fig. 2). From 1962 and until 1976, amplitudes were measured on paper records (SEFRAM). In 1976, the ML was defined and the previous amplitude measurements were reevaluated thanks to the magnetic records and the new data continued to be measured on paper and estimated with magnetic records. In 1996, the seismic acquisition and processing became entirely numerical.

3.3.1.2 Magnitude ML accuracy

To assess the uncertainties associated to the determination of ML, we consider the same dataset of 25 279 earthquakes with ML estimation and located not further than 20 km from the borders, as in the Section 3.2. We first recall that ML is calculated only on the LDG seismic stations (Tab. 1). Indeed, the several tens of additional stations from other seismic networks that can contribute to the epicenter location never contribute to the magnitude determination.

In Figure 5, we represent the normalized cumulative distribution of the number of stations used to compute the event magnitude ML, which is the arithmetic mean of the individual station magnitudes. It shows that for half of the earthquakes, the ML is computed on 4 or less stations. However, we emphasize on the fact that most of these earthquakes are very small and are therefore only recorded by few stations. If one takes into account the 5904 ML ≥ 2.0 earthquakes and the 422 ML ≥ 3.0 earthquakes, the median value reaches 10 and 32 stations respectively. The mean standard deviation for the whole dataset is 0.26 whereas it slightly exceeds 0.31 for ML ≥ 3.0. Indeed, ML ≥ 3.0 earthquakes are recorded on a large number of stations, which might increase the standard deviation due to the integration of attenuation heterogeneity on large distance.

3.3.2 Duration magnitude MD

As mentioned above, the local magnitude (ML) is only determined for epicentral distances larger than 95 km.
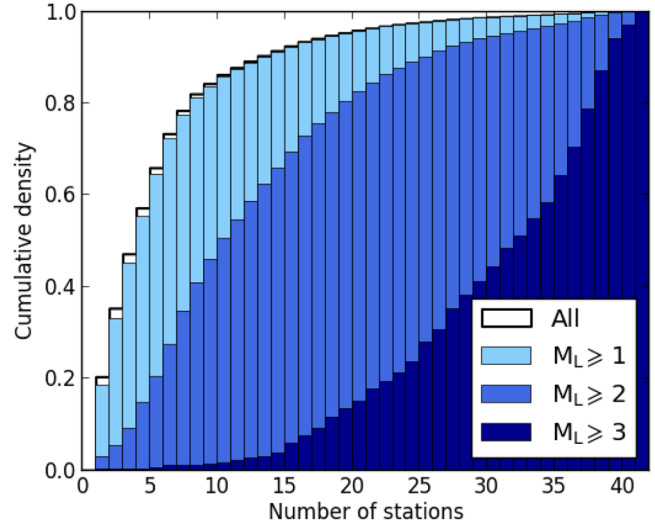

Fig. 5. Number of stations used to compute ML. Cumulative densities for earthquake recorded between 2010 and 2019 not further than 20 km from the French borders or coastlines. The cumulative density of all earthquakes is in black, ML ≥ 1 in light blue, ML ≥ 2.0 in royal blue and ML ≥ 3.0 in dark blue.

However, very small earthquake are not recorded beyond that distance, due to their too low signal-to-noise ratio at such distance. A duration magnitude (MD), based on the duration of the Lg wave is then calculated. This MD was defined in 1977, at the same time as the ML. At that time, the main objective was to be able to determine a magnitude when the seismic signal is saturated and therefore prevented from computing a ML. The general formulas are the following:

$-$ for $MD < 4.0$: $MD = A1 + A2\,log_{10}(t) + A3\Delta,$

$-$ for $MD \geq 4.0$: $MD = B1 + B2\log_{10}(t) + B3\,t^2 + B4\Delta,$
where

- t is the duration of the signal in seconds;
- Δ is the epicentral distance in kilometers;
- A1, A2, A3, B1, B2, B3 and B4 coefficients are station-dependent.

At that time, the LDG also showed that:

$$MD = ML_{LDG} + 0.06 \pm 0.27,$$

$$MD = mb_{USGS} \pm 0.25.$$

In 2002, it was decided to reevaluate the various coefficients in order to integrate new seismic stations. As a result, the LDG defined new formulas for MD in which coefficients A2, A3, B2, B3 and B4 were the same for all stations whereas A1 and B1 remained station-dependent. Then:

$$A2 = 1.665 \pm 0.005,$$

$$A3 = 0.0004 \pm 0.00001,$$

$$B2 = 1.714 \pm 0.011,$$

$$B3 = 0.486 * 10^{-6} \pm 0.16 * 10^{-7},$$

$$B4 = 0.467 * 10^{-3} \pm 0.967 * 10^{-5}.$$

Finally, in the same time, the LDG showed that:

$$MD = ML_{LDG} - 0.07 \pm 0.28. \qquad (3.1)$$

Figure S7 shows the correlation between magnitudes ML and MD of earthquakes that occurred during the period 2010–2019. It represents 23 929 earthquakes having both magnitude estimates and located not further than 20 km from the French borders or coastlines. However, it is important to note that, for this time period, most of MD are measured at very few stations: more than 75% of events have an estimation of MD at only one or two stations. Moreover, we notice that more than 50% of measurements have been made on five specific stations of the LDG network, which are MBDF, LPL and LPG located in the Alps, and ETSF and EPF in the Pyrenees. This can be explained by the fact that these regions concentrate many small events which are only seen at these few close stations. Nevertheless, in Figure S7, one can see an adequacy of the relation between ML and MD performed in 2002 (Eq. (3.1)) with recent seismic data. The ML-MD relation regressed for the 2010–2019 dataset is:

$$MD = ML_{LDG} + 0.01 \pm 0.21. \qquad (3.2)$$

Then, if a ML measurement is not possible, we could reasonably use the MD value to deduce an estimation of ML. During the 2010–2019 period, about 4500 earthquakes have an estimation of MD but no ML. It represents 16% of earthquakes recorded by the LDG during that period on the same spatial footprint, and these magnitudes MD range from 0.1 to 2.7. However, these events with a MD only have not been used in the following.

3.3.3 Moment magnitude Mw

For seismic hazard assessment, the common magnitude used is the moment magnitude (Mw), because Mw was designed to characterize the size of large earthquakes (Kanamori, 1977) and due to the development of many ground motion prediction equations (GMPE) in Mw. A catalogue of seismicity with homogeneous magnitudes covering a long time period is also a crucial input for probabilistic seismic hazard assessment (PSHA).

In this context, the SiHex project (Cara *et al.*, 2015) was launched in 2009 in France in order to determine Mw in a systematic way, even if the French seismicity is dominated by small earthquakes. In this framework, relations between ML from the LDG and Mw have been developed (Cara *et al.*, 2017). These conversion laws are based on the Mw obtained thanks to the analysis of crustal coda waves (Denieul *et al.*, 2015) of the larger and well constrained events. The Mw-ML relations obtained in the SiHex project are:

$$Mw = \alpha ML_{LDG} + \beta,$$

with coefficients defined as the following:
- for $ML > 4$: $\alpha = 0.8208$ and $\beta = 0.0804$
- for $3.117 \leq ML \leq 4$: $\alpha = 1$ and $\beta = -0.6$
- for $ML < 3.117$: $\alpha = 0.6642$ and $\beta = 0.4467$

Figure S8 represents this piecewise linear regression law with its standard deviation according to Cara *et al.* (2017).

In this paper, we do not work on the Mw and globally remain on the ML estimation for statistics and seismicity analyses over the last 10 years. However, some Mw based on coda-waves have been estimated by the LDG for the largest earthquakes as well as Mw obtained from full waveform inversions. These new data may provide more constrains in the conversion laws and improve the magnitude homogeneity through seismic catalogues.

4 Seismicity: bulletins and catalogue

4.1 Overview

The LDG earthquake catalogue consists of a list of seismic events detected by the national seismic network. These events are extracted from a seismic database documented among others with relocated hypocenters, in which non-natural events have been discriminated (Nicolas *et al.*, 1998). The largest earthquakes with $ML \geq 3.0$, which occurred since 1962, are shown in Figure 6. They represent only about 4% of the total number of earthquakes detected by the LDG network since its inception.

Regarding the metropolitan France extended with a buffer of 20 km from the French borders and coastlines, the LDG catalogue contains 25 265 earthquakes with a genuine ML, for the period 2010–2019 (Fig. 7 and Tab. S3). It represents 47% of the earthquakes recorded since 1962 with a genuine ML within the same area, in only 10 years. This is mainly due to the network capabilities' improvement that allowed the detection of smaller magnitude events. Local magnitude values range from ML 0.2 to 5.4. Among them, 427 events have $ML \geq 3.0$, including 29 events with $ML \geq 4.0$ and 4 events with $ML \geq 5.0$ (Tab. 4). Figure 8 shows magnitude histograms for the whole 10-year period as well as their temporal distribution. We also detail the earthquake magnitude distribution and spatio-temporal repartition for each year between 2010 and 2019 in the Text S1 and Figure S9.

Although we can get good estimation of the accuracy of epicentral locations, the hypocentral depths have to be taken into account with greater care. Indeed, depths are rarely well constrained and often set at 2 km for the shallowest earthquakes (Fig. 7). However, despite these difficulties, the systematic confrontation of the event depths with local networks optimally distributed above the seismicity (*e.g.* Perrot *et al.*, 2005; Cushing *et al.*, 2008; Got *et al.*, 2011; Theunissen *et al.*, 2018) suggests that the first order variations of the hypocentral depths of earthquakes at the scale of the territory appear to be interpretable.

Figure 7 shows that the average hypocentral depths are not homogeneous over the country. Indeed, the seismicity appears
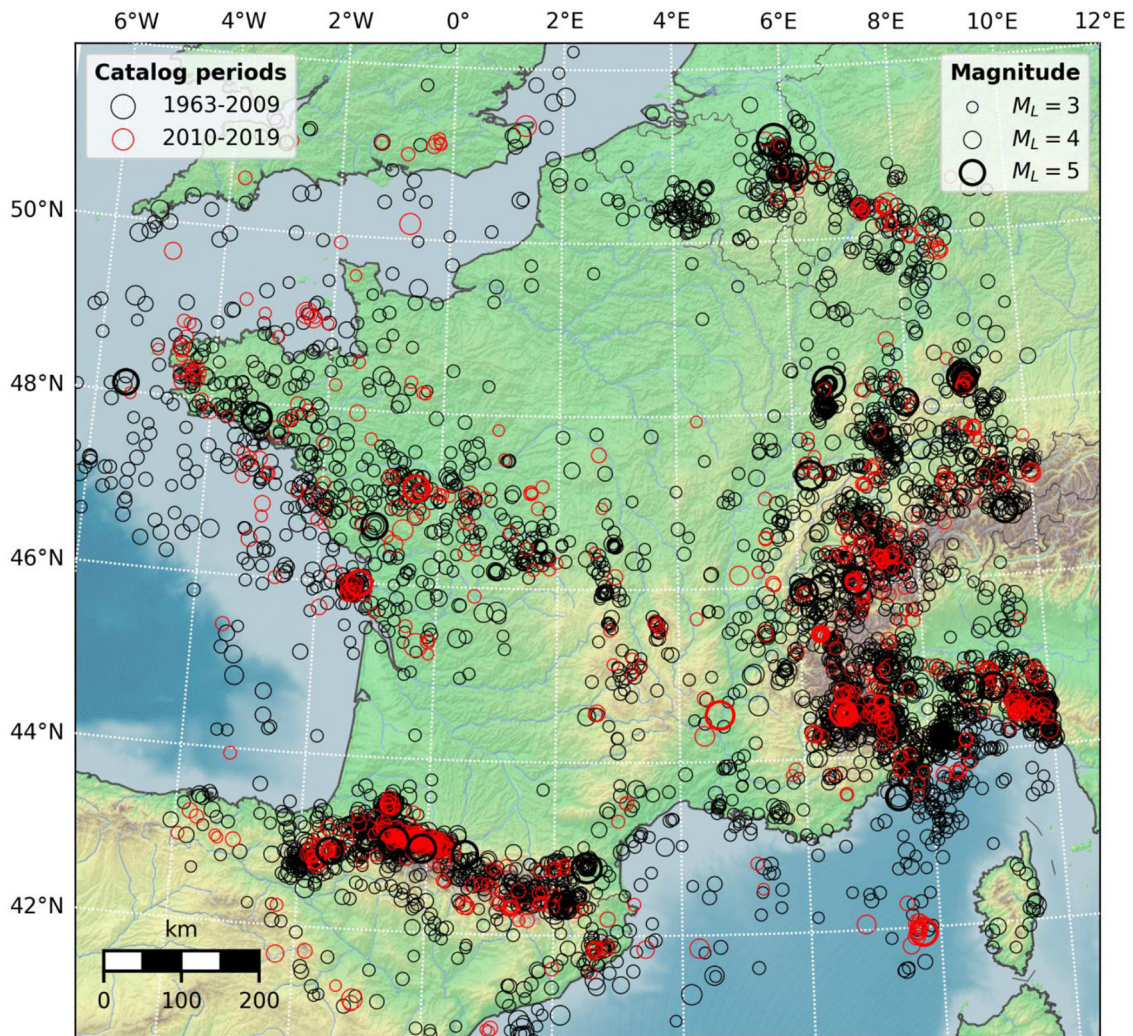
Fig. 6. Map of ML ≥ 3.0 earthquakes recorded by the LDG from 1963 to 2019. Black circles correspond to earthquakes occurred from 1963 to 2009 and red circles to earthquakes occurred from 2010 to 2019. A buffer of 200 km from the French borders and coastlines has been set to represent them.

to go down to 20 km depth in the Armorican Massif in the northwestern part of France, close to the Central Massif in the center part of France, and around the Vosges in the northeastern part of France. These three regions correspond to ancient crystalline massifs. We also notice deeper seismicity along the Rhine Graben. The earthquake mean hypocentral depth in these latter regions is greater than 7 km. In the youngest mountains belts of the Alps or the Pyrenees, the seismicity is globally shallower with a hypocentral mean depth of about 4 km. However the Pyrenees present the whole range of depths from the near-surface to some tens of kilometers explained by its geological history (Theunissen *et al.*, 2018).

A large difference between the ML and the Mw is often observed for earthquakes in western France (Tab. 4). The most likely explanation is that the crustal attenuation is lower there than in the rest of the territory (*e.g.* Campillo and Plantet, 1991; Mayor *et al.*, 2018). We remind here that the attenuation law used by the LDG was determined after the Friuli (eastern Italian Alps) seismic crisis that occurred in 1976–77 and weighted significantly on the attenuation law determination (MS 6.5 followed by 34 earthquakes of magnitude > 4.2, Aoudia *et al.*, 2000).

4.2 Magnitude-frequency distribution

The magnitude of completeness of the catalogue evolves with time due to the network densification and the improvement of the instruments and methodologies. Figure 9 shows the event density by ML between 1962 and 2019. It illustrates the progressive decrease of the completeness magnitude from about 3.5 to 2.0 and even a bit less than 2.0 nowadays. For the period 2010–2019, we estimate a completeness magnitude around 1.8, a magnitude value above the peak in number of events per magnitude bin (Fig. 9). The associated Gutenberg–Richter law showing the cumulative number of seismic events as a function of magnitude yields a b-value of 1.05 ± 0.01 using the Weichert (1980) algorithm. This value is typical of those obtained for background seismicity looking at large surface area, covering heterogeneous tectonic styles (*e.g.* Frohlich and Davis, 1993; Kagan, 1999; Petruccelli *et al.*, 2019). One can
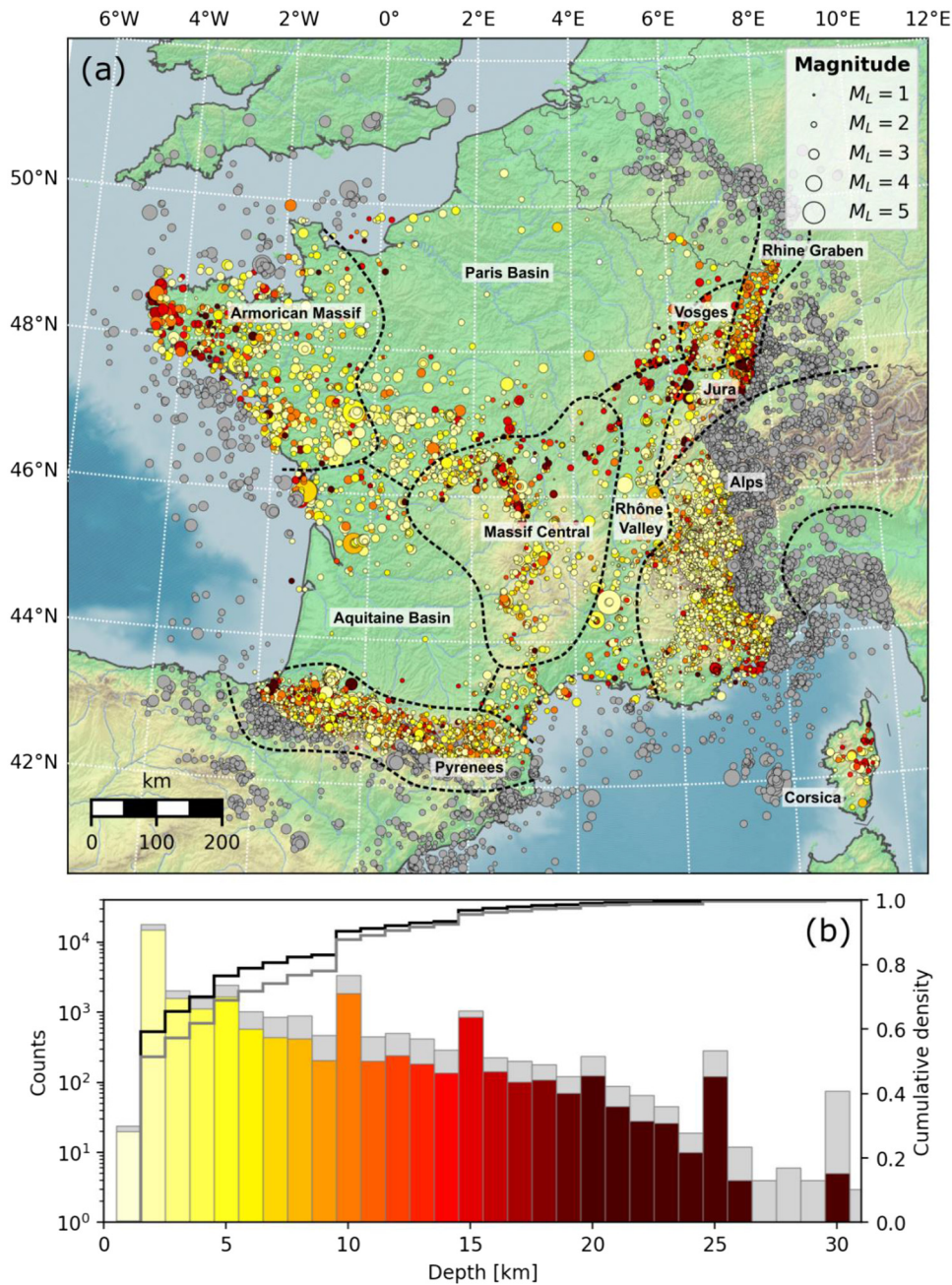
Fig. 7. Hypocenters of earthquakes recorded by the LDG from 2010 to 2019. (a) Map of earthquakes with a ML that occurred from 2010 to 2019. Color scale is related to the hypocentral depth. Colored earthquakes are located within the metropolitan France or not further than 20 km from the French borders and coastlines ("metropolitan EQs"). See also Table S3. Grey earthquakes are located between 20 km and 200 km from the French borders and coastlines ("distant EQs"). These earthquakes are not located inside mainland France or Corsica but are informative for the French seismic hazard. (b) Histogram of earthquake depths with count in log-scale. Color bars correspond to metropolitan EQs and grey bars include distant EQs. Black line is the cumulative density of metropolitan EQs as a function of depth. Grey line is the cumulative density including distant EQs.

note that it has been estimated without declustering the catalogue beforehand, unlike what is the common practice for properly estimating the seismic activity rate in a region for seismic hazard computation. Indeed, earthquakes that occur in clusters like swarms or aftershock sequences are usually removed from catalogues prior to being used in seismic hazard assessment because they could over predict the occurrence rate of fault ruptures in a specific area. Although the declustering step is quite important in seismic hazard, we do not discuss further this aspect, as it is not the scope of this study.

Table 4. Characteristics of ML ≥ 4.0 earthquakes. Columns are identifier number (ORID), date (yyyy-mm-dd) and time UTC (hh:mm:ss), latitude (°), longitude (°), depth (km) and local magnitude (ML). The table is ordered according to ML, from the largest to the smallest.

ORID	Date (yyyy-mm-dd)	Time UTC (hh:mm:ss)	Latitude (°)	Longitude (°)	Depth (km)	ML
5020509	2019-11-11	10:52:46	44.5373	4.6524	2	5.4
312508	2014-04-07	19:26:59	44.5206	6.6340	7	5.1
5016538	2019-06-21	06:50:58	47.1225	−0.4125	5	5.1
349779	2016-04-28	06:46:50	45.9973	−1.2799	7	5.1
5013759	2019-03-20	09:56:43	45.3128	−0.3125	8	4.9
270798	2012-02-26	22:37:55	44.5214	6.6981	8	4.8
289643	2012-12-30	23:35:02	43.0921	−0.1994	2	4.8
307164	2013-11-21	09:53:06	47.6926	−2.8268	4	4.6
369502	2017-03-10	06:43:34	42.9050	−1.6494	12	4.6
313380	2014-04-29	07:03:25	43.0599	0.0397	10	4.5
250067	2010-09-28	11:29:40	45.9540	−1.4243	2	4.5
387299	2018-02-12	03:08:31	46.6379	−0.6097	2	4.5
245044	2010-04-01	01:36:40	42.9749	0.2681	15	4.3
262143	2011-08-03	01:36:14	44.2989	4.3997	4	4.3
339512	2015-11-06	04:03:05	44.4714	6.7301	2	4.3
247444	2010-06-30	11:53:45	45.4104	6.4743	2	4.2
350063	2016-05-02	10:36:58	47.0651	0.4975	2	4.2
247432	2010-06-30	07:15:15	46.4675	−0.7559	3	4.2
349458	2016-04-25	04:44:09	43.4612	−0.6240	12	4.2
5010233	2018-11-21	17:08:55	46.1500	5.0149	2	4.2
271147	2012-03-02	07:15:51	44.4896	6.7060	10	4.2
350581	2016-05-11	10:45:53	43.1360	−0.6305	10	4.1
5015784	2019-05-28	08:48:07	46.3424	6.7743	2	4.1
289754	2013-01-05	23:26:12	43.0689	−0.2160	2	4.1
303960	2013-09-02	12:36:37	43.4443	−0.5924	2	4.1
382425	2017-10-28	19:06:13	42.8151	0.2403	2	4.0
5006794	2018-08-06	20:49:13	43.0361	0.3158	2	4.0
270876	2012-02-27	16:31:21	44.4784	6.6735	10	4.0
289816	2013-01-07	04:20:24	44.7675	6.6373	7	4.0

4.3 Significant earthquakes from 2010 to 2019

The five most significant earthquakes from these last 10 years are the 2019 ML 5.4 Le Teil earthquake, the 2019 ML 5.1 Lys-Haut-Layon earthquake, the 2019 ML 4.9 Montendre earthquake, the 2016 ML 5.1 La Rochelle earthquake, and the 2014 ML 5.1 Barcelonnette earthquake (Fig. 10). For each of these earthquakes, we discuss the LDG locations, magnitude estimations, and source focal mechanisms obtained using first-motion polarities or full waveform inversions (Tab. 5). The details of full waveform moment tensor inversions for each earthquake are further documented in the Text S2.

4.3.1 Le Teil (2019)

The Le Teil earthquake occurred on November 11, 2019 at 10 h 52 UTC (11 h 52 LT). Characterized by a local magnitude of ML 5.4, this earthquake is the largest seismic event recorded in metropolitan France in the last 10 years. The maximal intensity reported by the Macroseismic Intervention Group (Sira, 2015) on the field is VII to VIII on the EMS98 scale, in the town of Le Teil (Sira *et al.*, 2020). Moreover, Causse *et al.* (2021) show that both numerical predictions of the ground

acceleration and *in-situ* observations of displaced objects converge toward estimates of an exceptional level of ground acceleration in the fault vicinity.

In the southeastern region, the regional seismicity generally localizes around the Moyenne Durance fault system (Fig. 10e). The last earthquake with a larger magnitude was the 1909 Lambesc event, with Mw considered between 5.5 and 6.1 (Baroux *et al.*, 2003; Stich *et al.*, 2005) that occurred approximately 100 km away from the Le Teil epicenter.

The first automatic hypocentral location given for the LDG seismic alert was calculated using 34 permanent stations of the LDG network. A revision of the location, based on the integration of various seismological networks such as RESIF allowed to better estimate the actual hypocenter, close to the Rouvière fault. Additional networks gave the opportunity to pick about 300 phases recorded on 145 stations, and therefore to lower the azimuthal gap to 38°.

The focal mechanism based on first polarities recorded at 17 stations from the LDG, RESIF, INGV, GEOSCOPE networks, indicates a reverse focal mechanism, and is in agreement with the one obtained by full waveform inversion, performed on ten RESIF and LDG regional stations (Fig. S10). The inverted depth lies around 1 km and the calculated moment magnitude is Mw 4.8 (Vallage *et al.*, 2021), which is in
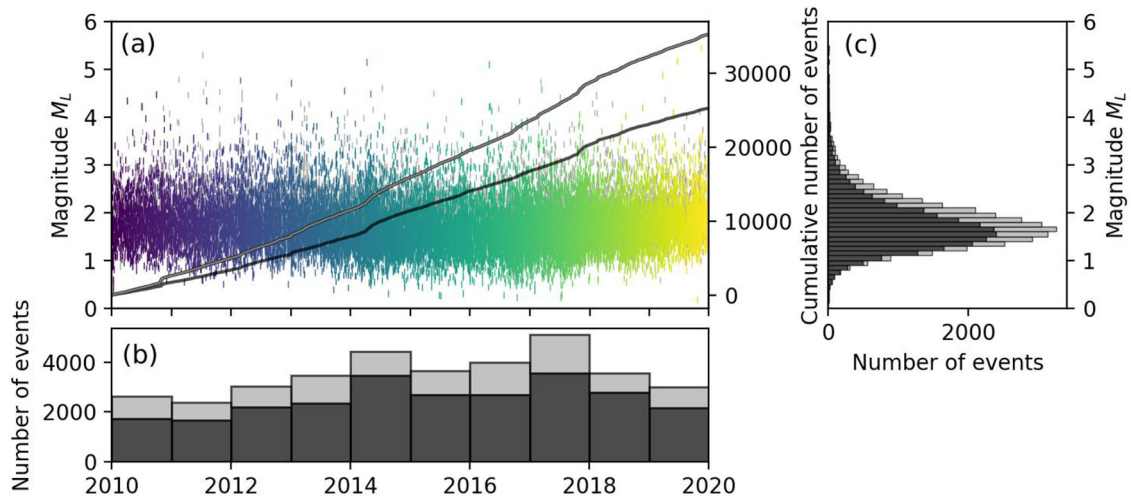
Fig. 8. Number of earthquakes and local magnitudes from 2010 to 2019. (a) Scatter plot of earthquake local magnitude (ML) as a function of time. Colored ticks correspond to earthquakes located within metropolitan France and not further than 20 km from the French borders and coastlines ("metropolitan EQs"). Color-scale is proportional to time. Black curve is the cumulative number of metropolitan EQs as a function of time. Grey ticks correspond to earthquakes located between 20 km and 200 km from the French borders and coastlines ("distant EQs"). Grey curve is the cumulative number of earthquakes including distant EQs as a function of time. (b) Histogram of the number of earthquakes per year. (c) Histogram of local magnitudes (ML). Black bars correspond to metropolitan EQs whereas grey bars include distant EQs.
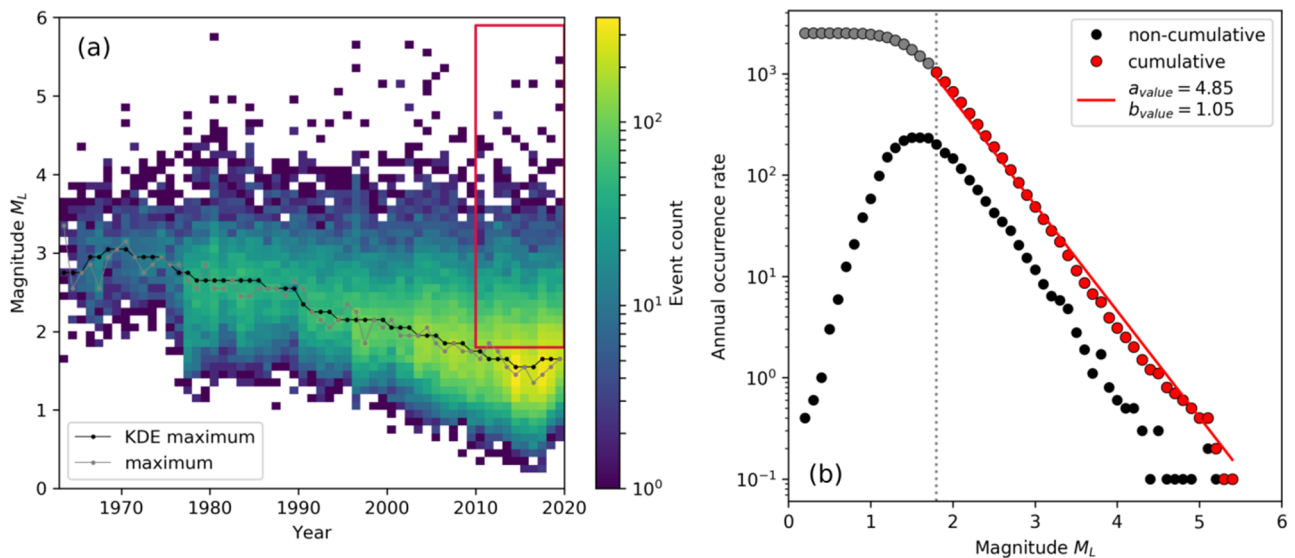

Fig. 9. Seismic activity and Gutenberg–Richter law. (a) Magnitude ML density per year. Grey line represents the magnitude bin with the maximum number of events for each year. Black line represents the magnitude bin with the KDE (Kernel Density Estimation) maximum number of events for each year. The red box indicates the period and data used to constrain the Gutenberg–Richter law on (b). (b) Gutenberg–Richter law for the period 2010–2019 (red line). The Weichert algorithm is used with a completeness magnitude of ML 1.8 (dotted vertical grey line). Black circles and red circles represent annual non-cumulative and annual cumulative number of earthquakes per magnitude bin, respectively.

agreement with other publications (Ritz *et al.*, 2020; Cornou *et al.*, 2021) and with rapid estimations from different French institutes such as OCA (Mw 4.9, 1 km) and IPGP (Mw 4.8, 3 km). The moment magnitude estimated from coda wave analysis at 14 LDG stations is slightly higher (Mw$_{coda}$ 5.2), in between the ML and the other moment magnitudes (Tab. 5). The strike of the focal mechanism (N 54°) roughly corresponds to the azimuth of the Rouvière fault.

Ultimately, InSAR measurements made with Sentinel 1 imagery clearly highlight surface deformation located on the Rouvière fault. The InSAR inversion revealed that the maximum amount of slip was localized at about 1 km depth and displacements were observed up to the surface (Ritz *et al.*, 2020; Vallage *et al.*, 2021).

The focal mechanisms, together with the geodetically identified fault, demonstrate that the earthquake reactivated as
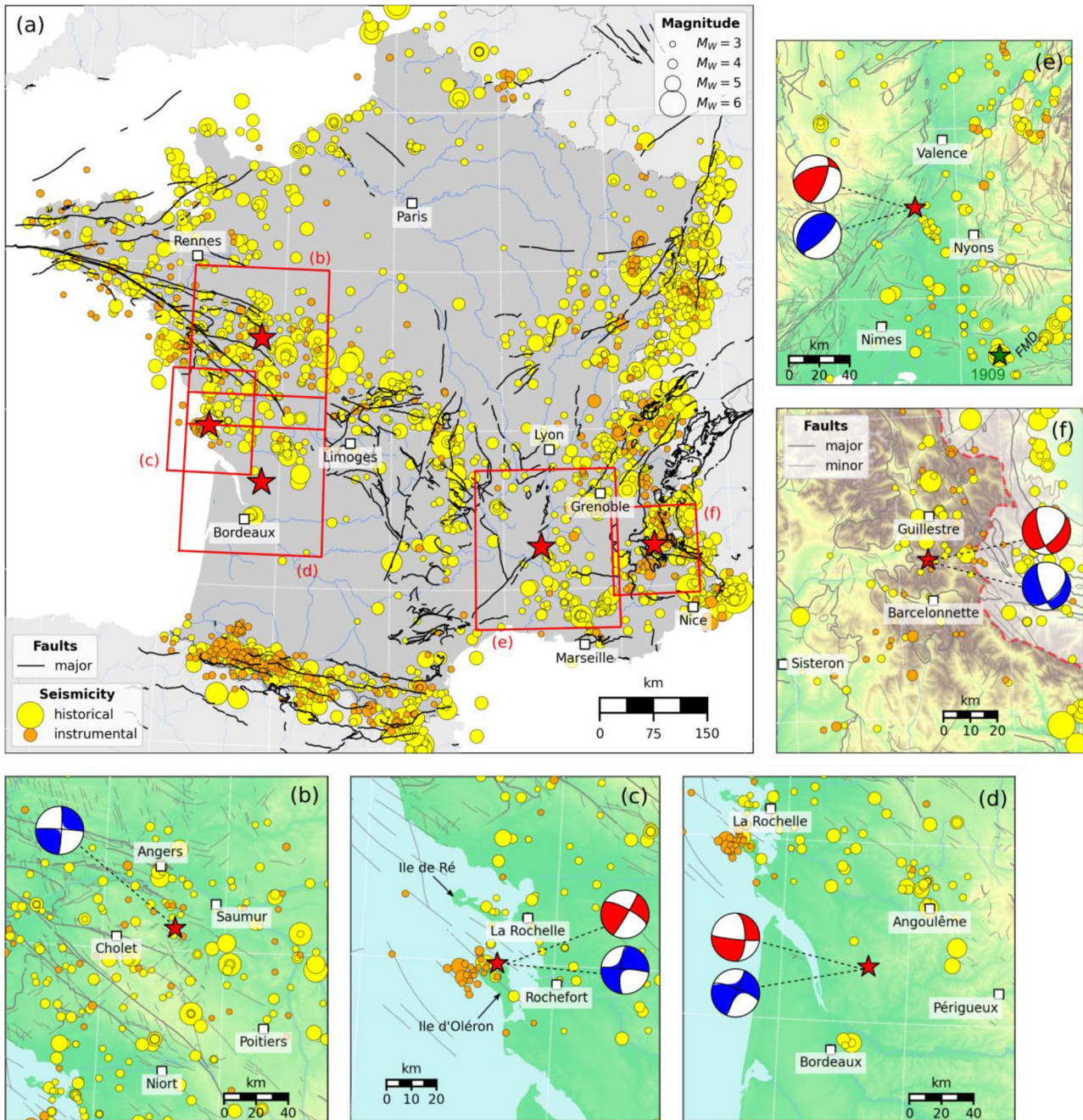
Fig. 10. The five most significant earthquakes from 2010 to 2019. (a) Map at national scale of the epicenters of the five most significant earthquakes (red stars), compared with location of the Mw ≥ 3 historical (yellow) and instrumental (orange) seismicity from FCAT-17 catalog (Manchuel *et al.*, 2018). This catalog covers the period 463 to 2009 merging the SisFrance historical macroseismic database (Scotti *et al.*, 2004) converted in Mw with calibrated intensity prediction equations (Baumont *et al.*, 2018; Traversa *et al.*, 2018), and the SiHex instrumental catalog (Cara *et al.*, 2015). The major faults are represented in black lines (Chantraine *et al.*, 1996). In subplots (b–f), focal mechanisms associated to the five most significant earthquakes are obtained either by polarity inversion of the first arrivals (red) or by full-waveform inversion (blue). The major faults (bold) and minor faults (thin) are represented with grey lines. (b) The ML 5.1 Lys-Haut-Layon earthquake on June 21, 2019. (c) The ML 5.1 La Rochelle earthquake on April 28, 2016. (d) The ML 4.9 Montendre earthquake on March 20, 2019. (e) The ML 5.4 Le Teil earthquake on November 11, 2019. Green star is the 1909 Lambesc earthquake. FMD is the Moyenne Durance Fault zone. (f) The ML 5.1 Barcelonnette earthquake on April 7, 2014. The red dashed line symbolizes the French-Italian border.

Table 5. Focal mechanism solutions and magnitude estimations. The identifier number (ID), the location, the first and second nodal planes with strike, dip, and rake, the depth, the local magnitude (ML), the duration magnitude (MD), the moment magnitude obtained from full-waveform tensor moment inversion (Mw inv), from coda waves (Mw coda) and from naive SiHex conversion (Mw SiHex) are presented for the five major earthquakes from 2010 to 2019. The table is ordered by occurrence dates from the most recent to the oldest. The first line of an earthquake presents the focal mechanism based on first-motion polarities (FMP) and the second line presents the results from the full waveform moment tensor inversions (FWI). The LDG velocity model was used for the inversion, presented in Table 2. The depth and moment magnitude are inverted and constrained by the model (see Text S2 for more information).

ID	Location		Nodal Plane 1 strike/dip/rake (°)	Nodal Plane 2 strike/dip/rake (°)	Depth (km)	ML	MD	Mw inv	Mw coda	Mw SiHex
5020509	Le Teil	FMP	021/61/55	256/44/136	2.0	5.4	4.9	–	5.2	4.6
		FWI	047/65/93	219/26/83	1.0	–	–	4.8	–	–
5016538	Lys-Haut-Layon	FMP	?	?	5.0	5.1	4.4	–	3.9	4.3
		FWI	272/85/173	003/83/5	6.0	–	–	3.9	–	–
5013759	Montendre	FMP	096/82/-144	000/54/-10	8.0	4.9	4.6	–	3.8	4.1
		FWI	022/88/18	291/72/178	9.0	–	–	3.8	–	–
349779	La Rochelle	FMP	298/68/173	031/84/22	7.0	5.1	4.5	–	?	4.3
		FWI	276/85/-162	184/72/-5	8.0	–	–	4.4	–	–
312508	Barcelonnette	FMP	162/63/-131	045/48/-38	7.1	5.1	4.9	–	4.8	4.3
		FWI	161/69/-127	045/42/-33	6.0	–	–	4.9	–	–

a thrust fault a steeply dipping NE-SW normal fault, which accommodated some extension during the Oligocene (Elmi *et al.*, 1996).

The very small number of aftershocks, only four recorded by the LDG stations in November, raised questions in the scientific community about the anthropogenic or tectonic origin of this event, also due to the close location of the event to a quarry (De Novellis *et al.*, 2020; Cornou *et al.*, 2021).

4.3.2 Lys-Haut-Layon (2019)

A ML 5.1 earthquake occurred on June 21, 2019 at 06:50 UTC (08:50 LT) between Saumur and Cholet (Fig. 10b) in Maine-et-Loire department. It is located about 28 km southwest of Saumur, 36 km east of Cholet and 40 km south of Angers. This event occurred in a zone of moderate seismic hazard. It was very broadly felt in western France, from Bordeaux to Normandy and from Rennes to Limoges. The BCSF collected more than 1200 testimonies in one hour but no damage was reported in the first hours after the earthquake. The intensities determined from the testimonies indicated a maximum intensity of VI on the EMS98 scale in the town of Tancoigné (Lys-Haut-Layon) at 6 km from the epicenter (Sira *et al.*, 2019).

A ML 2.8 aftershock was recorded about 9 minutes later. In 24 h, 11 aftershocks were detected by the LDG with magnitudes ranging from 1.7 to 3.0. This ML 5.1 Lys-Haut-Layon event is the strongest earthquake in more than 50 years in the region. From the late 1960s to the present, 25 earthquakes of magnitude greater than 3.0 occurred within a radius of 20 km around the epicenter. None of them exceeded the magnitude 3.9. Historically, within a radius of 100 km around the epicenter, two earthquakes of MSK intensity greater than or equal to VII (SisFrance) occurred: the October 6, 1711 earthquake at Loudun (86) of intensity VII–VIII and the January 9, 1772 earthquake at Parthenay (79) of intensity VII–VIII.

The inversion of the event mechanism indicates a strike-slip motion (Fig. 10b). It is consistent with past event mechanisms in the region (Nicolas *et al.*, 1990; Haugmard, 2016). It corresponds either to a left-lateral strike-slip motion along a N-S fault or to a right-lateral slip along an E-W fault. Bonnin *et al.* (2019) installed a post-seismic seismic network and detected more than one hundred aftershocks spatially distributed along E-W direction, suggesting a right-lateral rupture along an E-W structure.

The earthquake focal depth is determined in the upper part of the crust, between 4 and 8 km. The regional moment tensor inversion (Fig. S11) gives a maximum waveform fit at a depth of 6 km. At this depth, the moment tensor indicates a magnitude Mw 3.9. This moment magnitude is in agreement with the Mw 3.9 determined using crustal coda waves (Denieul *et al.*, 2015) at 13 LDG stations, or the Mw 3.9 at 7 km depth obtained by Geoazur with FMNear method (Delouis, 2014) or even the Mw 3.9 obtained by the IPGP with SourceSpec (https://github.com/SeismicSource/sourcespec) method based on spectral analysis.

4.3.3 Montendre (2019)

The 2019 Montendre earthquake occurred in the southern part of the Charente Maritime department, in a region called the Saintonge, on the East side of the Gironde Estuary (Fig. 10d). Seismically, it is a region of transition between the La Rochelle-Rochefort-Oléron area with its moderate seismicity and the very low rates of instrumental seismicity of the Aquitanian basin. This region was affected by a significant earthquake on March 20, 2019 at 09:56 UTC that was felt within a radius of approximately 200 km (Sira *et al.*, 2019). The intensities reached V at three sites between Montendre and Jonzac (Sira *et al.*, 2019) about 60 km North from Bordeaux.

The hypocenter was determined using 202 arrival times but is associated to a 111° azimuthal gap due to its location near the west coast. With no station at short distance, the earthquake

focal depth was not well resolved and was forced by analysts to 8 km, a depth in agreement with the best depth obtained by moment tensor inversion (between 7 and 11 km and with a maximum variance reduction at 9 km, Fig. S12).

The LDG location is distant of about 5 km to the North of the RENASS location, and of the macroseismic epicentral area. The local magnitude was estimated at ML 4.9, a value significantly higher than the estimated moment magnitude Mw 3.8 (Tab. 5), obtained either by moment tensor inversion (Fig. S12) or by coda wave analysis at 11 stations. Such magnitude discrepancy between ML and Mw is commonly observed in metropolitan France, and especially in the western region due to the local attenuation (Denieul *et al.*, 2015).

Five aftershocks of ML 2.3 to 3.5 were detected slightly eastward within 15 km in the next 16 days, two of them at close distance within 6 h. Their locations are not sufficient to help determine the orientation of the fault plane activated by the event. The focal mechanisms of the earthquake deduced from the first arrival polarities and the full waveform inversion are in good agreement (Fig. 10d) and show almost a purely strike-slip faulting with WNW-ESE and NNE-WSW nodal planes.

Given the hypocentral depth, the earthquake occurred in the basement, which is known to be highly faulted/fractured at depth, within a broad NW-SE shear zone. A few NW-SE faults, slightly oblique, affecting the sedimentary cover, were mapped in the vicinity (including the Jonzac anticlinorium, Platel *et al.*, 1975). However, no definitive association between the earthquake at depth and the trace of the faults could be determined.

4.3.4 La Rochelle (2016)

The La Rochelle earthquake occurred at 06 h 46 UTC (8 h 46 LT) on April 28, 2016. It was felt at Bordeaux (130 km), Limoges (190 km) and Rennes (240 km) and even farther, up to 300 km from the epicenter (Sira *et al.*, 2016). With intensities up to VI (at Angoulins – Charente Maritime, from BCSF) between La Rochelle and Rochefort (Fig. 10c), both affected by intensity V as within a 30 km wide region around the I_{max}, this was the most damaging earthquake of the region since the 1970s (Sira *et al.*, 2016). Its local magnitude estimated at ML 5.1 is, as for the Montendre earthquake, significantly higher than its moment magnitude (Mw 3.9).

Despite the large number of stations used for phase pickings (300), the azimuthal gap remained high (73°) due to the earthquake's coastal location. The shortest epicentral distance remained large too (70 km). Its depth was forced by analysts to 7 km, a value that appears slightly shallower than the depth of 10.3 km determined at teleseismic distance by picking pP and sP depth phases. The hypocentral location is therefore associated to a significant uncertainty (significantly larger than the 1.4 km-long error ellipse determined). This partly explains the differences (up to 15 km with the EMSC) in term of epicentral location with other institutes.

Despite the uncertainty on the final location, the epicenter falls in the 15 km-large strait of Pertuis d'Antioche, between the Ré and Oléron islands (Fig. 10c). The earthquake therefore lied close to other past Oléron earthquakes, and in particular in the vicinity of the September 7, 1972 earthquake (I_{max} VII). This 1972 event is the largest regional recorded mainshock, and is significantly larger than the 2016 event, whose

magnitude was estimated at Mw 5.0 compared to Mw 3.9 for the 2016 one (Cara *et al.*, 2015).

The earthquake focal mechanism, derived from the polarities of the first arrivals, appears to indicate a strike-slip fault motion with NW-SE and NE-SW nodal planes similar to the 1972 earthquake. The moment tensor inversion suggests that the nodal planes are more E-W and N-S (Fig. S13). These focal mechanisms, complemented with others associated with the 1977–1978 and 1984 earthquakes (Nicolas *et al.*, 1990), are consistent with the principal orientation of the largest tectonic structures that affect the basement in the area (Fig. 10c). Indeed, most of the faults are NW-SE oriented, with minor N-S oriented planes like within a C-S structural fabric, within a crustal shear zone which develops south from the south Armorica shear zone.

The LDG observation is consistent with a scenario involving a reactivation of an Hercynian inherited fault plane. Nonetheless, a more precise association of the earthquake to a given fault remains impossible due to the significant uncertainty on the hypocentral location of the earthquake and to the absence of known aftershocks.

4.3.5 Barcelonnette (2014)

One moderate earthquake of ML 5.1 occurred on April 7, 2014 about 15 km North of Barcelonnette (Fig. 10f). Relatively shallow, this earthquake was widely felt in the epicentral region, as well as throughout the southeast part of France within a 300 km radius. It caused only minor damages in the epicentral area, such as some chimney fallings leading to reported intensities between II and VI and an epicentral intensity estimated at $I_0 = V$–VI on the EMS98 scale (Sira *et al.*, 2014).

The 2014 Barcelonnette hypocenter was obtained using more than 240 phase-picks (with Pg, Sn, Sg) at a total of 116 stations. The primary and secondary azimuthal gaps are rather small (30° and 35° respectively). The major axis of the error ellipse is about 1.2 km. However, the focal depth remained poorly resolved at regional distances, the closest station MBDF being at 25 km from the epicenter. A focal depth of 7–8 km was obtained from pP and sP (depth) phases at teleseismic distances.

Focal mechanisms (Fig. 10f) were determined using two approaches, firstly thanks to polarities of the first arrivals and secondly with full-waveform inversion. Both solutions are characteristic of an extensive regime, associated to a fault with a large normal component and a small dextral component. These focal mechanisms obtained by the LDG agreed with others determined by Geoazur, Sismalp, GFZ, INGV and USGS, and are consistent with the principal orientation of the largest tectonic structures, which constitute the Serrene fault system.

The best solution of the full-waveform inversion of the moment tensor gives a Mw 4.9 at 7 km depth (Fig. S14). The moment magnitude was also estimated using the methodology of Denieul *et al.* (2015) from crustal coda waves. This Mw_{coda} 4.8 corresponds to the preferred moment magnitude published by the BCSF (Sira *et al.*, 2014). The ML and Mw estimations give here much more similar magnitude values, since the ML (LDG) definition mainly relies on records of earthquakes occurred in the Alps.
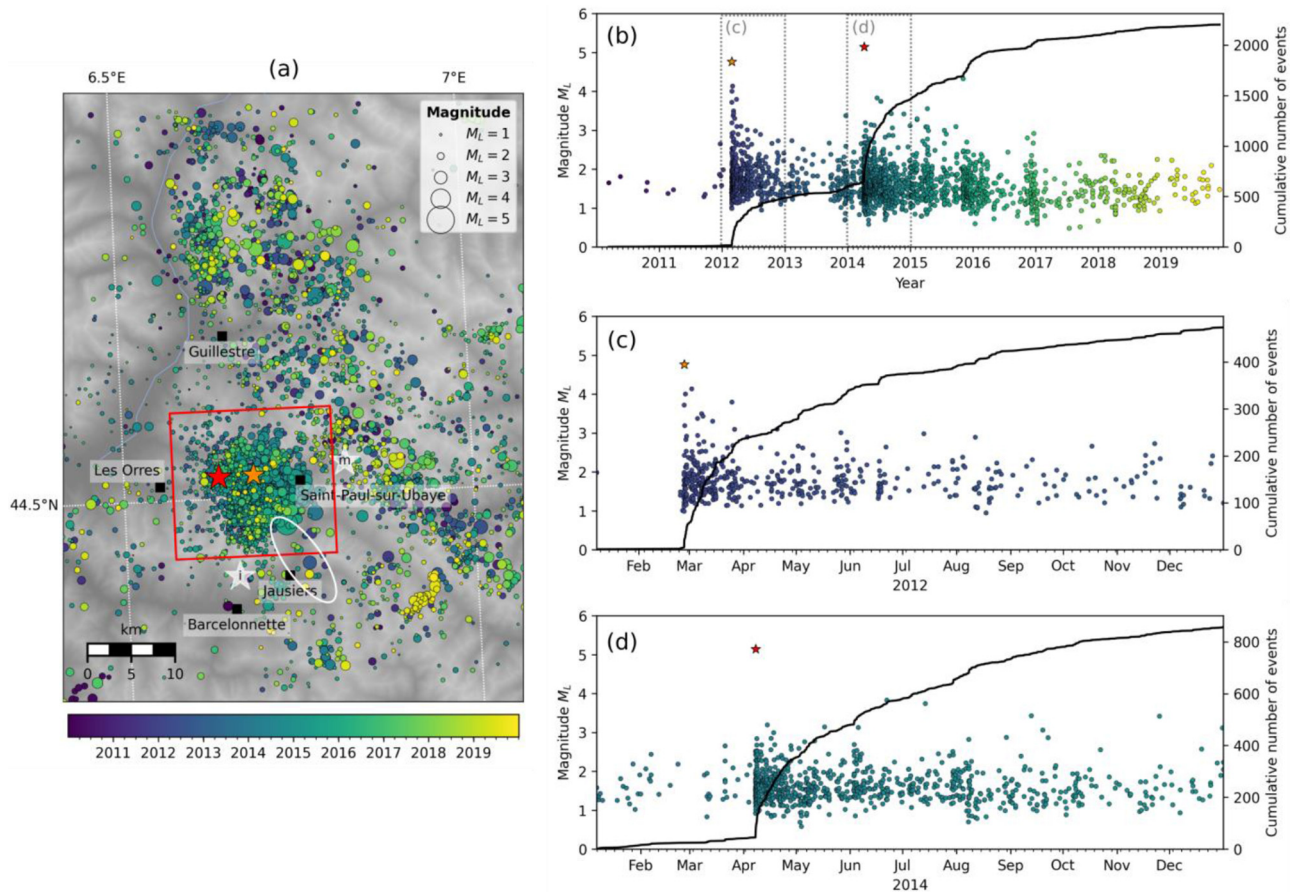
Fig. 11. The Barcelonnette cluster. (a) Map of the seismicity from 2010 to 2019 in the Ubaye valley. The red frame highlights the location of Barcelonnette cluster and defines the selected earthquakes for the next subplots. Orange and red stars are the 2012 and 2014 mainshocks respectively. The two white stars indicate the macroseismic (m) and the instrumental (i) location of the April 5, 1959 earthquake (Nicolas *et al.*, 1998). The white ellipse represents the extension of the 2003–2004 seismic swarm. (b) Cumulative number of earthquakes from 2010 to 2019 and magnitude distribution in time. (c) Zoom on the cumulative number of earthquakes and magnitudes in 2012. (d) Zoom on the cumulative number of earthquakes and magnitudes in 2014.

This earthquake is the most significant one occurring in the Alps since the July 15, 1996 ML 5.3 Epagny earthquake near Annecy (Thouvenot *et al.*, 1998), with $Mw_{(SiHex)}$ 4.9, which had a larger impact on the population due to the higher population density. Its epicentral location is also close to the historical April 5, 1959 earthquake located around Saint-Paul-sur-Ubaye (Fig. 11a), with ML 5.3 (Nicolas *et al.*, 1998), $Mw_{(FCAT-17)}$ 5.1 and an epicentral intensity of VII–VIII (SisFrance), one of the largest recorded in the Ubaye valley. We discuss and focus on the cluster behavior of the seismicity within this area, in the next section.

4.4 Swarms and mainshock-aftershock sequences

4.4.1 Ubaye valley (southern French Alps)

The Ubaye valley, in the French Alps, is known for its numerous seismic crises (*e.g.* Jenatton *et al.*, 2007; Thouvenot *et al.*, 2016) and suffered from two moderate earthquakes during these last 10 years (Fig. 11). The first one of ML 4.8 occurred on February 26, 2012, was felt within a 200 km radius around the epicenter (Sira *et al.*, 2012), and generated a substantial earthquake cluster. The second one is the ML 5.1

occurred on April 7, 2014 (described in the previous section), which reactivated the same cluster. The two epicenters are separated by less than 1 km, and their focal mechanisms showed very similar extensive NW-SE oriented structures (Courboulex *et al.*, 2013; Thouvenot *et al.*, 2016). They located a few kilometers northwest from the 2003–2004 swarm largely detailed by Jenatton *et al.* (2007) and also relatively close to the epicentral zone of one of the largest earthquakes of the last century (April 5, 1959, ML 5.3, Nicolas *et al.*, 1998) in the French Alps (Fig. 11a).

These 2012 and 2014 mainshocks were both followed by thousands of aftershocks. The total time series of this 2012–2015 cluster counted about 13 000 earthquakes detected by the closest stations (Thouvenot *et al.*, 2016). Most of the aftershocks located by LDG are concentrated in a narrow circle of about 10-km-diameter at crustal depths (roughly between 1 and 5 km). After the ML 4.8 earthquake in February 2012, 10 aftershocks of ML ≥ 3.0 were recorded by the LDG within the first two months. After the ML 5.1 earthquake in April 2014, six ML ≥ 3.0 aftershocks, two in April, one in May, two in June and one in July 2014 were recorded by the LDG. The temporal distributions of earthquakes look like typical
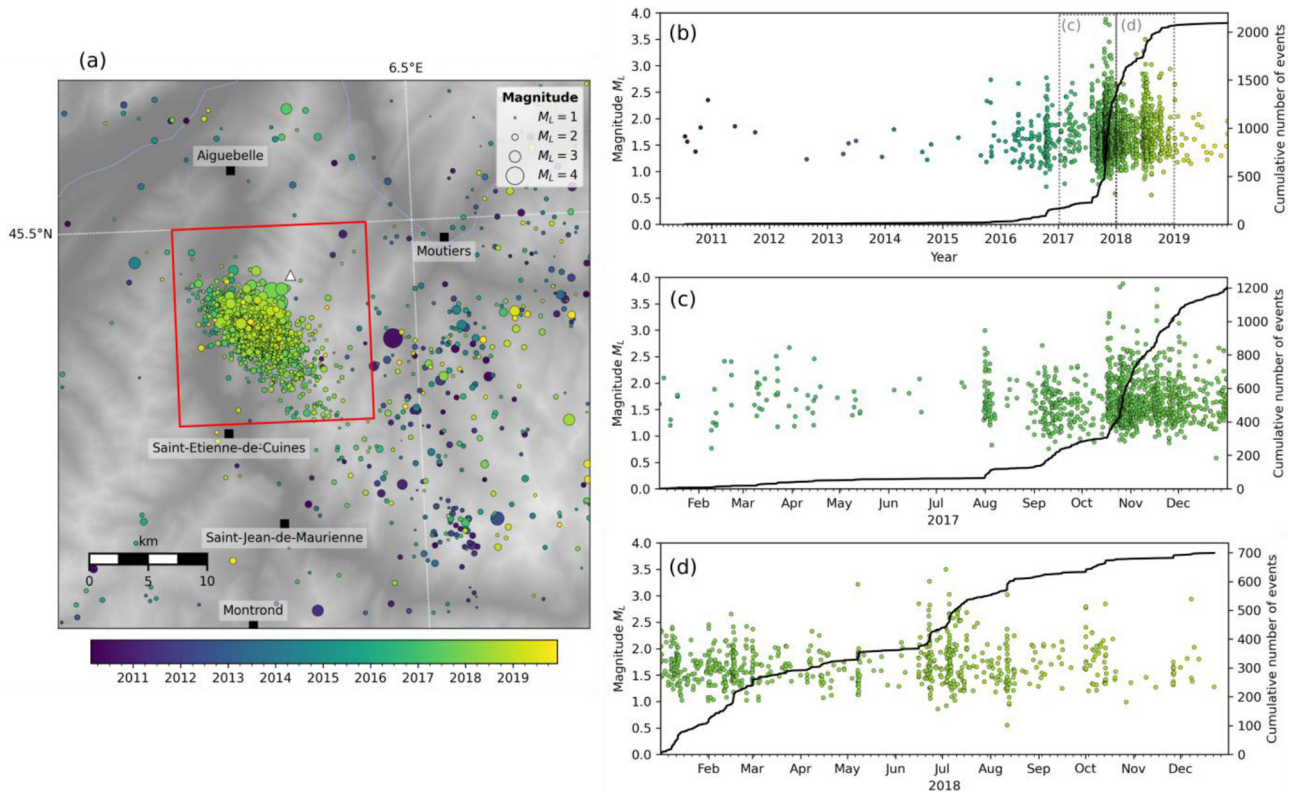
Fig. 12. The Maurienne swarm. (a) Map of the seismicity from 2010 to 2019. The red frame highlights the location of Maurienne swarm and defines the selected earthquakes for the next subplots. The white triangle indicates the highest peak of the Lauzière Massif culminated at 2829 m. (b) Cumulative number of earthquakes from 2010 to 2019 and magnitude distribution in time. (c) Zoom on the cumulative number of earthquakes and magnitudes in 2017. (d) Zoom on the cumulative number of earthquakes and magnitudes in 2018.

mainshock-aftershocks sequences following Omori power law decays (Figs. 11c and 11d) with a *p*-value of 0.95 in 2012 and a p-value of 1.0 in 2014, considering 100 days after each mainshock (Fig. S15). However, earthquake interactions in the Ubaye valley are much more complicated (Thouvenot *et al.*, 2016; De Barros *et al.*, 2019) with mixed behaviors including swarm-type often related to fluids (*e.g.* Jenatton *et al.*, 2007; Daniel *et al.*, 2011; Leclère *et al.*, 2013; Fojtíková and Vavryčuk, 2018) and classical tectonic aftershock sequences.

These earthquake clusters illuminate fault systems affecting the cover and/or basement. The seismic activity reflects either the tectonic activity or the fluid diffusion, or both. Indeed, the seismicity could be fluid-driven, related to pore-pressure diffusion and hydro-fracturation but could also reflect transient slip events related or not to fluids (*e.g.* Ruhl *et al.*, 2016; Duverger *et al.*, 2018; Hoste-Colomer *et al.*, 2018; De Barros *et al.*, 2020).

4.4.2 Maurienne valley (northern French Alps)

A long-lasting seismic swarm occurred between fall 2015 and fall December 2019 (Fig. 12) in the Maurienne valley, in Savoy. The epicentral zone, located between Aiguebelle to the North and Saint-Etienne-de-Cuines to the South beneath the Lauzière massif, was not known for any particular instrumental seismic activity before 2015. However, historical testimonies from the 19th century documented a previous swarm in the region, which threatened the local population (Rothé, 1938).

This swarm lasted from December 1838 to June 1844 with plenty of testimonies between 1838 and 1840, and was approximately centered beneath the village of Montrond (Billiet, 1851), south of Saint-Jean-de-Maurienne (Fig. 12a).

The recent Maurienne swarm was particularly active during 2017 and 2018 (Figs. 12c and 12d) with approximately 2000 events detected and located by the LDG with local magnitude ML(LDG) ranging from 0.5 to 3.9. The maximum magnitude event of ML 3.9 occurred on October 27, 2017, ten days after a real increase of the number of earthquakes per day and just two days after a ML 3.8 event. Another ML 3.8 occurred on November 17, 2017. The swarm activity started decreasing softly in December 2017 but increased again mid-2018 with a ML 3.5 event on July 3. Finally, the seismic activity tapered off at the end of 2019 (Fig. 12b). This swarm differed from a mainshock-aftershock sequence because the largest earthquakes occur days after the seismic crisis initiation.

In Belledonne crystalline massif, fault scarps at the Rognier Mountain, a few kilometers southwest from the swarm, that were previously interpreted as resulting from tectonic activity (Bordet, 1970) have been re-interpreted as counter-slope scarps related to the development of a system of post-glacial gravitational faults (Hippolyte *et al.*, 2006). The poor resolution of the depth of the hypocenters from the national network precludes demonstrating whether those events could be related to the sackung (gravitational collapse of the flanks of the mountain following the retreat of glaciers) or to deeper seated faults.

5 Discussion: implication for seismic hazard assessment

As previously mentioned, the updates of the earthquake catalogue with the seismicity that occurred from 2010 to 2019 contribute to 47% of the total number of natural earthquakes in the LDG database. This addition is therefore substantial, contributing to:

1 A few more moderate earthquakes felt by many people. These realizations give the potential to revise some regional historical events that occurred in their vicinity. In addition, these events documented by hundreds of macroseismic observations will also help tying better intensity predictive attenuation models (*e.g.* Bakun and Scotti, 2006; Baumont *et al.*, 2018; Provost and Scotti, 2020). The strong ground motion records, associated to the earthquake coordinates and magnitude also add data to the discussions on the regional differences in the source stress parameters (Ameri *et al.*, 2017). Finally, these earthquakes help document the present day stress field heterogeneities, as well as possible associations with fault planes, which is crucial for improving physics based works, giving the possibility, among others, to evaluate stress transients on activated receiver fault planes and estimating the regional stress field expressions to tectonic and surface loads (*e.g.* Craig *et al.*, 2016).

2 Many small earthquakes. The large number of earthquakes due to better detection capacity leads to a lower completeness magnitude of the catalogue and helps analyze their spatiotemporal variations (see Sect. 4.4). The resultant better knowledge of the time structure of the seismicity helps constrain the processes responsible for some seismic clusters (De Barros *et al.*, 2019). The larger number of earthquakes helps determine more robust frequency-magnitude distributions, and enables the mapping of the b-values spatiotemporal variations. These frequency-magnitude distributions are crucial for the PSHA, but complex due to the low seismicity rates and heterogeneities (Beauval and Scotti, 2003). Finally, given the larger number of records every year, more events occur at small distances from seismic stations, giving the potential to resolve more regularly their hypocentral depths which is an important parameter.

Updates of the seismicity catalogues, with a better resolution of the depth, of the rate and spatio-temporal variations of earthquakes and eventual association with given faults and strong motion attenuation impact the boundaries and parameters of the seismotectonic zoning scheme (*e.g.* Baize *et al.*, 2013; Drouet *et al.*, 2020). This in turn affects the main input of the DSHA and PSHA models.

This recent instrumental seismicity makes it possible to revisit the historical seismicity and to bring new complementary information in order to better constrain its parameters. At first order, latest earthquakes do not imply major revisions of our knowledge; however the new contributions in term of earthquake depths, eventual relations with tectonic structures, or other source characteristics help better documenting the seismogenic behavior of the metropolitan crust. In addition,

these data participate in the reduction of uncertainties associated to the seismic hazard parameters, and allow decisions to be made using more robust hypothesis testing (*e.g.* Vallage and Bollinger, 2019; Beauval *et al.*, 2020).

The LDG produces weekly bulletins and a national catalog of metropolitan seismicity using a methodology unchanged since 1962. This catalog creates a good starting point for French seismic hazard studies but needs to be complemented by more specific and detailed local studies. During the last decade, the metropolitan seismicity has been documented by a whole bunch of local or regional analyses (*e.g.* Got *et al.*, 2011; Chevrot *et al.*, 2011; Souriau *et al.*, 2014; Theunissen *et al.*, 2018; De Barros *et al.*, 2019; Ritz *et al.*, 2020) and including sequence of earthquakes triggered or induced (*e.g.* Bollinger *et al.*, 2010; Lengliné *et al.*, 2017; Aochi and Burnol, 2018; Grasso *et al.*, 2018; Maurer *et al.*, 2020), while some other authors revisited historical observations thanks to more robust processing sometimes helped by recent data acquisition (*e.g.* Traversa *et al.*, 2018; Kaub *et al.*, 2021; Amorèse *et al.*, 2020). In the same time, publications on local or regional data should highlight useful information for engineering purpose and applied research in order to facilitate their integration in seismic hazard models. Altogether with the national and long-lasting LDG observations, they participate to a better interpretation of the uncertainties on seismic hazard inputs.

6 Conclusion and perspectives

More than 50 000 seismic events were recorded by the LDG during these last ten years in metropolitan France and its surroundings. This number is significantly larger than what was recorded in the prior decades. Most of the differences come from the seismological network evolution and improvements, and do not reflect an increase of the natural earthquake activity. The number of $ML \geq 3$ earthquakes per year is approximately stable with an annual mean of about 40 earthquakes. During the period 2010–2019, the French territory was struck by 29 events of $ML \geq 4$, and among them, three of the five largest earthquakes occurred in 2019. More than 90% of hypocentral depths are shallower than 15 km, but remain often under-constrained due to both the low-to-moderate magnitude of recorded seismic events and the spatial repartition of the stations that span the whole metropolitan territory. Regarding the seismicity of $ML \geq 3$, 61% of epicenters are accurate to within 5 km with a 90% confidence level (figures coming from GT5 criteria).

Seismic data recorded by the LDG between 2010 and 2019 can significantly enrich the national catalogues available today and help the transition toward the complete seismic national network of RESIF. However, to be done correctly, well documented workflows are necessary both to interpret local and regional data, and to merge them into a national model needed for seismic hazard assessment. The LDG network installed since the early 1960s and the LDG catalogue benefitting from a continuous increase in completeness over more than 40 years with a decrease of one magnitude unit, these data allow a better characterization of the temporal structure of seismicity, partly diffuse, and in the form of mainshock-aftershocks sequences or transient swarms. These aspects are important to better estimate the seismic hazard in

metropolitan France. As perspectives, we plan to explore the impact of these recent and numerous seismic event records on the French seismic hazard or more exactly on the possible reduction of uncertainties associated to seismic hazard models.

Supplementary Material

Table S1. Characteristics of the high-gain seismograph stations of the LDG network since 1962.
Table S2. Other networks operational from 2010 to 2019 and used for locations.
Table S3. The LDG catalogue for the period 2010–2019.
Table S4. Global GT5 criteria.

Figure S1. Earthquake waveforms.
Figure S2. Quarry blast waveforms.
Figure S3. Marine explosion waveforms.
Figure S4. Landslide waveforms.
Figure S5. Phase time residuals and Vp/Vs.
Figure S6. Ground-motion attenuation.
Figure S7. Magnitudes MD vs ML.
Figure S8. Magnitude Mw vs ML.
Figure S9. Annual earthquake activity.
Figure S10. Full-waveform inversion of the 2019 Le Teil earthquake.
Figure S11. Full-waveform inversion of the 2019 Lys-Haut-Layon earthquake.
Figure S12. Full-waveform inversion of the 2019 Montendre earthquake.
Figure S13. Full-waveform inversion of the 2016 La Rochelle earthquake.
Figure S14. Full-waveform inversion of the 2014 Barcelonnette earthquake.
Figure S15. Omori's laws for the Barcelonnette cluster in 2012 and 2014.

Text S1. Annual earthquake activity from 2010 to 2019.
Text S2. Moment tensor inversions (Saikia, 1994; Dreger, 2003; Masson *et al.*, 2019; Mazzotti *et al.*, 2020; Mazzotti *et al.*, 2021).

The Supplementary Material is available at http://www.bsgf.fr/10.1051/bsgf/2021014/olm.

References

Ameri G, Drouet S, Traversa P, Bindi D, Cotton F. 2017. Toward an empirical ground motion prediction equation for France: Accounting for regional differences in the source stress parameter. *Bulletin of Earthquake Engineering* 15(11): 4681–4717.

Amorèse D, Benjumea J, Cara M. 2020. Source parameters of the 1926 and 1927 Jersey earthquakes from historical, instrumental, and macroseismic data. *Physics of the Earth and Planetary Interiors* 300: 106420.

Aochi H, Burnol A. 2018. Mechanism of the M L 4.0 25 April 2016 earthquake in southwest of France in the vicinity of the Lacq gas field. *Journal of Seismology* 22(5): 1139–1155.

Aoudia A, Saraò A, Bukchin B, Suhadolc P. 2000. The 1976 Friuli (NE Italy) thrust faulting earthquake: a reappraisal 23 years later. *Geophysical Research Letters* 27(4): 573–576.

Baize S, Cushing EM, Lemeille F, Jomard H. 2013. Updated seismotectonic zoning scheme of Metropolitan France, with reference to geologic and seismotectonic data. *Bulletin de la Société Géologique de France* 184(3): 225–259.

Bakun WH, Scotti O. 2006. Regional intensity attenuation models for France and the estimation of magnitude and location of historical earthquakes. *Geophysical Journal International* 164: 596–610.

Baroux E, Pino N, Valensise G, Scotti O, Cushing, M. 2003. Source parameters of the 11 June 1909, Lambesc (Provence, southeastern France) earthquake: A reappraisal based on macroseismic, seismological, and geodetic observations. *Journal of Geophysical Research: Solid Earth* 108(B9).

Baumont D, Manchuel K, Traversa P, Durouchoux C, Nayman E, Ameri G. 2018. Intensity predictive attenuation models calibrated in Mw for metropolitan France. *Bulletin of Earthquake Engineering* 16(6): 2285–2310.

Beauval C, Scotti O. 2003. Mapping b-values in France using two different magnitude ranges: Possible non power-law behavior. *Geophysical Research Letters* 30(17).

Beauval C, Bard PY, Danciu L. 2020. The influence of source-and ground-motion model choices on probabilistic seismic hazard levels at 6 sites in France. *Bulletin of Earthquake Engineering* 18 (10): 4551–4580.

Belinić T, Markušić S. 2017. Empirical criteria for the accuracy of earthquake locations on the Croatian territory. *Geofizika* 34(1): 1–17.

Billiet A. 1851. Mémoire sur les tremblements de terre ressentis en Savoie. *Mémoires de l'Académie Royale de Savoie* XIII: 245–282.

Bollinger L, Nicolas M, Marin S. 2010. Hydrological triggering of the seismicity around a salt diapir in Castellane, France. *Earth and Planetary Science Letters* 290(1-2): 20–29.

Bondár I, McLaughlin KL. 2009. A new ground truth data set for seismic studies. *Geophysical Research Letter* 80: 465–472.

Bondár I, Myers SC, Engdahl ER, Bergman EA. 2004. Epicentre accuracy based on seismic network criteria. *Geophysical Journal International* 156: 483–496.

Bonnin M, Beucler E, Fligiel D, Gernigon P, Kouadio K, Mocquet A. 2019. Sismicité dans le quart Nord-Ouest de la France métropolitaine état des lieux du réseau et premiers résultats. In: *4e rencontres RESIF, 12–14 novembre 2019*.

Bordet P. 1970. Les failles vivantes du massif des Grands Moulins (Massif cristallin externe de Belledonne). *Géologie Alpine* 46: 43–47.

Campillo M, Plantet J-L. 1991. Frequency dependence and spatial distribution of seismic attenuation in France: experimental results and possible interpretations. *Physics of the Earth and Planetary Interiors* 67(1-2): 48–64.

Cara M, Cansi Y, Schlupp A, Arroucau P, Béthoux N, Beucler E, *et al.* 2015. SI-Hex: a new catalogue of instrumental seismicity for metropolitan France. *Bulletin de la Société Géologique de France* 186(1): 3–19.

Cara M, Denieul M, Sèbe O, Delouis B, Cansi Y, Schlupp A. 2017. Magnitude Mw in metropolitan France. *Journal of Seismology* 21 (3): 551–565.

Causse M, Cornou C, Maufroy E, Grasso J-R, Baillet L, El Haber E. 2021. Exceptional ground motion during the shallow Mw 4.9 2019 Le Teil earthquake, France. *Communications Earth & Environment* 2: 14.

Chantraine J, Autran A, Cavelier C, Clozier L. 1996. Carte géologique de la France à l'échelle du millionième. BRGM, Service géologique national.

Chatelain JL, Roecker SW, Hatzfeld D, Molnar P. 1980. Microearthquake seismicity and fault plane solutions in the Hindu Kush region and their tectonic implications. *Journal of Geophysical Research: Solid Earth* 85(B3): 1365–1387.

Chevrot S, Sylvander M, Delouis B. 2011. A preliminary catalog of moment tensors for the Pyrenees. *Tectonophysics* 510(1-2): 239–251.

Cornou C, Ampuero J-P, Aubert C, Audin L, Baize S, Billant J, *et al.* 2021. Rapide response to the Mw 4.9 earthquake of November 11, 2019 in Le Teil, Lower Rhône Valley, France. *Compte-Rendu Géosciences*, preprint: https://doi.org/10.31219/osf.io/3afs5.

Courboulex F, Dujardin A, Vallée M, Delouis B, Sira C, Deschamps A, *et al.* 2013. High-Frequency Directivity Effect for an Mw 4.1 Earthquake, Widely Felt by the Population in Southeastern France. *Short Note. Bulletin of the Seismological Society of America* 103 (6): 3347–3353.

Craig TJ, Calais E, Fleitout L, Bollinger L, Scotti O. 2016. Evidence for the release of long-term tectonic strain stored in continental interiors through intraplate earthquakes. *Geophysical Research Letters* 43(13): 6826–6836.

Cushing EM, Bellier O, Nechtschein S, Sébrier M, Lomax A, Volant P, *et al.* 2008. A multidisciplinary study of a slow-slipping fault for seismic hazard assessment: the example of the Middle Durance Fault (SE France). *Geophysical Journal International* 172(3): 1163–1178.

Daniel G, Prono E, Renard F, Thouvenot F, Hainzl S, Marsan D, *et al.* 2011. Changes in effective stress during the 2003–2004 Ubaye seismic swarm, France. *Journal of Geophysical Research: Solid Earth* 116(B1).

De Barros L, Baques M, Godano M, Helmstetter A, Deschamps A, Larroque C, *et al.* 2019. Fluid-Induced Swarms and Coseismic Stress Transfer: A Dual Process Highlighted in the Aftershock Sequence of the 7 April 2014 Earthquake (Ml 4.8, Ubaye, France). *Journal of Geophysical Research: Solid Earth* 124(4): 3918–3932.

De Barros L, Cappa F, Deschamps A, Dublanchet P. 2020. Imbricated aseismic slip and fluid diffusion drive a seismic swarm in the Corinth Gulf, Greece. *Geophysical Research Letters* 47.

De Novellis V, Convertito V, Valkaniotis S, Casu F, Lanari R, Tobar M, *et al.* 2020. Editorial Expression of Concern: Coincident locations of rupture nucleation during the 2019 Le Teil earthquake, France and maximum stress change from local cement quarrying. *Communication Earth & Environment* 1: 37.

Deichmann N, Clinton J, Husen S, Edwards B, Haslinger F, Fäh D, *et al.* 2012. Earthquakes in Switzerland and surrounding regions during 2011. *Swiss Journal of Geosciences* 105(3): 463–476.

Delouis B. 2014. FMNEAR: Determination of focal mechanism and first estimate of rupture directivity using near-source records and a linear distribution of point sources. *Bulletin of the Seismological Society of America* 104(3): 1479–1500.

Denieul M, Sèbe O, Cara M, Cansi Y. 2015. Mw from crustal coda waves recorded on analog seismograms. *Bulletin of Seismological Society of America* 105(2A): 831–849.

Dreger DS. 2003. TDMT_INV: Time Domain Seimsic Moment INVersion. *International Handbook of Earthquake and Engineering Seismology* 81B: 1627.

Drouet S, Ameri G, Le Dortz K, Secanell R, Senfaute G. 2020. A probabilistic seismic hazard map for the metropolitan France. *Bulletin of Earthquake Engineering* 18(5): 1865–1898.

Duverger C, Lambotte S, Bernard P, Lyon-Caen H, Deschamps A, Nercessian A. 2018. Dynamics of microseismicity and its relationship with the active structures in the western Corinth Rift (Greece). *Geophysical Journal International* 215(1): 196–221.

Elmi S, Busnardo R, Clavel B, Camus G, Kieffer G, Bérard P, *et al.* 1996. Notice explicative, Carte Géologique France 1/50 000, feuille Aubenas (865). Orléans : BRGM.

Fojtíková L, Vavryčuk V. 2018. Tectonic stress regime in the 2003–2004 and 2012–2015 earthquake swarms in the Ubaye Valley, French Alps. *Pure and Applied Geophysics* 175(6): 1997–2008.

Frohlich C, Davis SD. 1993. Teleseismic b values; or, much ado about 1.0. *Journal of Geophysical Research: Solid Earth* 98(B1) 631–644.

Geiger H. 1910. The scattering of α-particles by matter. *Proceedings of the Royal Society of London. Series A, Containing Papers of a Mathematical and Physical Character* 83(565): 492–504.

Grasso JR, Karimov A, Amorese D, Sue C, Voisin C. 2018. Patterns of Reservoir-Triggered Seismicity in a Low-Seismicity Region of France. *Bulletin of the Seismological Society of America* 108 (5B): 2967–2982.

Got JL, Monteiller V, Guilbert J, Marsan D, Cansi Y, Maillard C, *et al.* 2011. Strain localization and fluid migration from earthquake relocation and seismicity analysis in the western Vosges (France). *Geophysical Journal International* 185(1): 365–384.

Haugmard M. 2016. Détermination non-linéaire des paramètres hypocentraux et structuraux: application à la sismicité intra-continentale du Massif armoricain. Doctoral dissertation, Université Bretagne Loire.

Hippolyte JC, Brocard G, Tardy M, Nicoud G, Bourlès D, Braucher R, *et al.* 2006. The recent fault scarps of the Western Alps (France): Tectonic surface ruptures or gravitational sackung scarps? A combined mapping, geomorphic, levelling, and 10Be dating approach. *Tectonophysics* 418(3-4): 255–276.

Hoste-Colomer R, Bollinger L, Lyon-Caen H, Adhikari LB, Baillard C, Benoit A, *et al.* 2018. Lateral variations of the midcrustal seismicity in western Nepal: Seismotectonic implications. *Earth and Planetary Science Letters* 504: 115–125.

Jenatton L, Guiguet R, Thouvenot F, Daix N. 2007. The 16 000-event 2003–2004 earthquake swarm in Ubaye (French Alps). *Journal of Geophysical Research: Solid Earth* 112(B11).

Kagan YY. Universality of the seismic moment-frequency relation. In: *Seismicity patterns, their statistical significance and physical meaning. Ed*. Basel (Switzerland): Birkhäuser, 1999, pp. 537–573.

Kanamori H. 1977. The energy release in great earthquakes. *Journal of Geophysical Research* 82(20): 2981–2987.

Kaub C, Geoffroy L, Bollinger L, Perrot J, Le Roy P, Authemayou C. 2021. Is the Machecoul fault the source of the ~M6 1799 Vendée earthquake (France)? *Geophysical Journal International* 225(3): 2035–2059.

Larsonnier F, Rouillé G, Bartoli C, Klaus L, Begoff P. 2019. Comparison on seismometer sensitivity following ISO 16063-11 standard. *International Congress of Metrology*. https://doi.org/10.1051/metrology/201927003.

Leclère H, Daniel G, Fabbri O, Cappa F, Thouvenot F. 2013. Tracking fluid pressure buildup from focal mechanisms during the 2003–2004 Ubaye seismic swarm, France. *Journal of Geophysical Research: Solid Earth* 118(8): 4461–4476.

Lengliné O, Boubacar M, Schmittbuhl J. 2017. Seismicity related to the hydraulic stimulation of GRT1, Rittershoffen, France. *Geophysical Journal International* 208(3): 1704–1715.

Manchuel K, Traversa P, Baumont D, Cara M, Nayman E, Durouchoux C. 2018. The French seismic CATalogue (FCAT-17). *Bulletin of Earthquake Engineering* 16(6): 2227–2251.

Marin S, Avouac JP, Nicolas M, Schlupp A. 2004. A probabilistic approach to seismic hazard in metropolitan France. *Bulletin of the Seismological Society of America* 94(6): 2137–2163.

Masson C, Mazzotti S, Vernant P, Doerflinger E. 2019. Extracting small deformation beyond individual station precision from dense Global Navigation Satellite System (GNSS) networks in France and western Europe. *Solid Earth* 10(6): 1905–1920.

Maurer V, Gaucher E, Grunberg M, *et al*. 2020. Seismicity induced during the development of the Rittershoffen geothermal field, France. *Geothermal Energy* 8: 5.

Mayor J, Traversa P, Calvet M, Margerin L. 2018. Tomography of crustal seismic attenuation in Metropolitan France: implications for seismicity analysis. *Bulletin of Earthquake Engineering* 16(6): 2195–2210.

Mazzotti S, Jomard H, Masson F. 2020. Processes and deformation rates generating seismicity in metropolitan France and conterminous Western Europe. *BSGF – Earth Science Bulletin* 191(1): 19.

Mazzotti S, Aubagnac C, Bollinger L, Coca Oscanoa K, Delouis B, Do Paco D, *et al*. 2021. FMHex20: A database of earthquake focal mechanisms in metropolitan France and conterminous Western Europe. *BSGF – Earth Sciences Bulletin*. https://doi.org/10.1051/bsgf/2020049.

Nicolas M, Santoire JP, Delpech PY. 1990. Intraplate seismicity: new seismotectonic data in Western Europe. *Tectonophysics* 179(1-2): 27–53.

Nicolas M, Béthoux N, Madeddu B. 1998. Instrumental seismicity of the Western Alps: a revised catalogue. *Pure and Applied Geophysics* 152: 707–731.

Perrey A. 1875. Note sur les tremblements de terre en 1871 avec suppléments pour les années antérieures, de 1843 à 1870. Ed. Hayez. vol. 24.

Perrot J, Arroucau P, Guilbert J, Déverchère J, Mazabraud Y, Rolet J, *et al*. 2005. Analysis of the Mw 4.3 Lorient earthquake sequence: a multidisciplinary approach to the geodynamics of the Armorican Massif, westernmost France. *Geophysical Journal International* 162(3): 935–950.

Petruccelli A, Schorlemmer D, Tormann T, Rinaldi AP, Wiemer S, Gasperini P, *et al.* 2019. The influence of faulting style on the size-distribution of global earthquakes. *Earth and Planetary Science Letters* 527: 115791.

Platel JP, Moreau P, Vouvé J, Colmont G. 1975. Notice explicative, Carte Géologique France 1/50 000, feuille Jonzac (731). Orléans : BRGM.

Provost L, Scotti O. 2020. QUake-MD: Open-source code to quantify uncertainties in magnitude–depth estimates of earthquakes from macroseismic intensities. *Seismological Research Letters* 91(5): 2520–2530.

Ritz J, Baize S, Ferry M, Larroque C, Audin L, Delouis B, *et al*. 2020. Surface rupture and shallow fault reactivation during the 2019 Mw 4.9 Le Teil earthquake, France. *Communications Earth and Environment* 1: 10.

Rothé JP. 1936. Les tremblements de terre en France en 1934. *Annuaire de l'Institut de Physique du Globe* 2: 88–110.

Rothé JP. 1938. Les séismes des Alpes françaises et la sismicité des Alpes occidentales. *Annales de l'Institut de Physique du Globe* 3: 1–105.

Ruhl CJ, Abercrombie RE, Smith KD, Zaliapin I. 2016. Complex spatiotemporal evolution of the 2008 Mw 4.9 Mogul earthquake swarm (Reno, Nevada): Interplay of fluid and faulting. *Journal of Geophysical Research: Solid Earth* 121(11): 8196–8216.

Saikia C. 1994. Modified frequency–wave number algorithm for regional seismo-grams using Filon's quadrature; modelling of Lg waves in eastern North America. *Geophysical Journal International* 118: 142–158.

Scotti O, Baumont D, Quenet G, Levret A. 2004. The French macroseismic database SISFRANCE: objectives, results and perspectives. *Annals of Geophysics*.

Sira C. 2015. Macroseismic Intervention Group: The Necessary Field Observation. In: Ansal A, (ed). *Perspectives on European Earthquake Engineering and Seismology*. Geotechnical, Geological and Earthquake Engineering, vol. 39. Cham: Springer.

Sira C, Schlupp A, Schaming M, Granet M. 2012. Séisme de Barcelonnette (Alpes de Haute Provence) du 26 février 2012. Rapport BCSF, 2012-R1, 43 p., 10 figures, 8 annexes.

Sira C, Schlupp A, Schaming M, Chesnais C, Cornou C, Dechamp A, *et al*. 2014. Séisme de Barcelonnette du 7 avril 2014. Rapport BCSF, 2014-R1, 76 p., 22 figures, 6 annexes.

Sira C, Schlupp A, Schaming M. 2016. Séisme de La Rochelle du 28 avril 2016. Rapport BCSF, 2016-R1, 82 p., 50 figures, 4 annexes.

Sira C, Schaming M, Delouis B, Satriano C. 2019. Séisme de Tancoigné du 21 juin 2019. Rapport sismologique BCSF-RENASS, 2019-R2, 47 p., 3 tableaux, 13 figures, 8 annexes.

Sira C, Schlupp A, Dretzen R, Schaming M, Maufroy E, Provost L, *et al*. 2020. Séisme du Teil du 11 novembre 2019. Rapport macrosismique BCSF-RENASS ; 2020-R2, 27 p.

Stich D, Batlló J, Macià R, Teves-Costa P, Morales J. 2005. Moment tensor inversion with single-component historical seismograms: The 1909 Benavente (Portugal) and Lambesc (France) earthquakes. *Geophysical Journal International* 162(3): 850–858.

Souriau A, Rigo A, Sylvander M, Benahmed S, Grimaud F. 2014. Seismicity in central-western Pyrenees (France): A consequence of the subsidence of dense exhumed bodies. *Tectonophysics* 621: 123–131.

Theunissen T, Chevrot S, Sylvander M, Monteiller V, Calvet M, Villaseñor A, *et al*. 2018. Absolute earthquake locations using 3-D versus 1-D velocity models below a local seismic network: example from the Pyrenees. *Geophysical Journal International* 212 (3): 1806–1828.

Thouvenot F, Fréchet J, Tapponnier P, Thomas JC, Le Brun B, Ménard G, *et al*. 1998. The ML 5.3 Epagny (French Alps) earthquake of 1996 July 15: a long-awaited event on the Vuache Fault. *Geophysical Journal International* 135(3): 876–892.

Thouvenot F, Jenatton L, Scafidi D, Turino C, Potin B, Ferretti G. 2016. Encore Ubaye: Earthquake Swarms, Foreshocks, and Aftershocks in the Southern French. *Bulletin of the Seismological Society of America* 106(5): 2244–2257.

Traversa P, Baumont D, Manchuel K, Nayman E, Durouchoux C. 2018. Exploration tree approach to estimate historical earthquakes Mw and depth, test cases from the French past seismicity. *Bulletin of Earthquake Engineering* 16(6): 2169–2193.

Vallage A, Bollinger L. 2019. Testing Fault Models in Intraplate Settings: A Potential for Challenging the Seismic Hazard Assessment Inputs and Hypothesis? *Pure and Applied Geophysics* 1–11.

Vallage A, Bollinger L, Champenois J, Duverger C, Guilhem Trilla A, Hernandez B, *et al.* 2021. Multi-technology characterisation of an unusual surface rupturing intraplate earthquake: The ML 5.4 2019 Le Teil event in France. *Geophysical Journal International*, ggab136, https://doi.org/10.1093/gji/ggab136.

Veinante-Delhaye A, Santoire JP. 1980. Sismicité récente de l'Arc Sud Armoricain et du Nord-Ouest du Massif Central. Mécanismes au foyer et tectonique. *Bulletin de la Société Géologique de France* 7(1): 93–102.

Weichert DH. 1980. Estimation of the earthquake recurrence parameters for unequal observation periods for different magnitudes. *Bulletin of the Seismological Society of America* 70(4): 1337–1346.